REPRINT 216

Stress analysis of thin shells of revolution under non-symmetric loads

By J. C. FALKENBERG
Norwegian Building Research Institute

NORWEGIAN BUILDING RESEARCH INSTITUTE

NBI

OSLO 1973

Ci 75

UDC 624.074.4:539.4
624.042

ACTA POLYTECHNICA SCANDINAVICA

CIVIL ENGINEERING AND BUILDING CONSTRUCTION SERIES No. 75

Stress analysis of thin shells of revolution under non-symmetric loads

J.C. FALKENBERG

Norwegian Building Research Institute, Blindern, Norway

HELSINKI 1973

Abstract

The differential equations for thin shells of revolution developed by Flügge are reviewed and arranged in a matrix form. Anisotropic properties and temperature strains are included. Equilibrium and compatibility equations for elastic rings of fairly arbitrary cross-section are established. Shell boundary conditions are formulated. An integration technique using a matrix series expansion is outlined. It has good numerical stability.

Computational examples include a hyperbolic cooling tower under wind, a skewly filled silo, a conical shell with point load, a ball valve housing and two spherical shells.

A brief outline of the RSHELL computer programme currently in operation is given.

Shells of revolution. Failure of the Ferrybridge Cooling Towers, 1st November 1965.

Table of contents

List of symbols

The following list includes the symbols which are used throughout the text. A number of other symbols are defined and used independently within each chapter. Bold types indicate vectors or matrices.

Shell

$\theta\ s\ z\ \phi$	coordinates	(Fig. 1)
$r\ r_1$	radii of curvature	(Fig. 1)
$u\ v\ w$	displacements	(Fig. 1)
$p q$	external loads and moments	(Fig. 3)
$\epsilon\ \gamma$	strains	
$\sigma\ \tau$	stresses	
$N M Q$	stress resultants	(Fig. 3)
E	modulus of elasticity	
ν	Poisson's ratio	
$D K$	extensional and bending stiffness	(Eqs. (21) and (22))
F	action vector	(Eq. (6))
S	stress resultants vector	(Fig. 3)

Ring

u	displacements	(Fig. 5)
p	loads	(Fig. 6)
ϵ	strains	
S	stress resultants	(Fig. 7)

Others

m	Fourier number	
mm	highest Fourier number	
A B	coefficient matrix and load vector	(Eq. (41))
J C	coefficient matrix and vector of constants for boundary conditions	(Eq. (74))
G L	transfer matrix and particular integral	(Eqs. (63) and (86))

1 Introduction

A great variety of engineering structures have the form of a thin-walled body of revolution. In the domain of civil engineering we find structures such as domes, chimneys and cooling towers, water storage tanks and silos; in the domain of mechanical engineering we have pressure vessels and pipeline accessories such as valves and couplings of various kinds, and aeronautical engineers make use of shells of revolution for rocket bodies. We should also mention some everyday appliances such as bottles and drinking glasses, which certainly play an important although not very spectacular part in our lives.

The engineering analysis, i.e. the calculation of stresses and deformations, in shells of revolution under loads, has received considerable attention from engineers and mathematicians.

Extensive bibliographies on the subject may be found in the works of FLÜGGE [1], BRØNDUM-NIELSEN [2] and BORN [3], to mention a few. These works all belong to the »pre-computer era of shell analysis» when the limitations of manual computation restricted the class of managable problems to fairly simple and regular shell shapes such as cylinders, cones and spheres, preferably with axisymmetric loading, although a number of non-symmetrical loading cases were also solved by analytic methods.

The linear analysis of shells of revolution belongs to that class of problems which can be transformed into a one-dimensional problem. This is so because all loading and response quantities, i.e. stresses and displacements, can be expanded in Fourier series in the circumferential direction. This leads to a set of ordinary differential equations for each harmonic.

The one-dimensional problem may then be handled by a finite-element technique, for which a number of computer codes have been written [4]. Alternatively, a finite-difference integration may be employed, for which computer codes also exist [4]. Both of these approaches involve introducing approximations, such as substituting pieces of straight lines or circular segments for the generating curve, or substituting differences for differentials.

For shells with relatively smooth geometry and loading such approximations may not have very significant effects on the results, but for more intricate shapes and loadings such approximations may have considerable effects and these techniques may require a very large number of nodal points for acceptable accuracy and hence prove quite costly with regard to preparation of input as well as with regard to computer time.

In contrast to the finite-element or finite different techniques, the integration methods on which the author's work is based do not involve any approximations of the above kinds, but employ a direct series expansion of the true coefficient matrices for the differential equations which are derived in an implicit form. Although basically very accurate, such a »transfer matrix» technique is not entirely trouble-free, as problems of numerical instability arise in certain cases. As anyone knows who has worked in the

field of computer analysis of structures, no one techniques is inherently trouble-free in all cases, in spite of the »complete generality» sometimes claimed by its author.

The methods and techniques to be described in the subsequent chapters have, however, proved useful for a number of quite complicated cases, and have the special merit of involving very little work for the preparation of input data. They are also rather economical with respect to computer storage and processing time.

The author's work on shells of revolution originated with the collapse of the Ferrybridge Cooling Towers in England in November 1965. The author, then a research student at Southampton University, was encouraged to undertake a bending analysis. The towers under wind forces had the form of thin hyperboloides of revolution.

It was during this effort, which was completed in March 1966 [5], that the computational technique was developed on which the present work is based.

The work subsequently underwent considerable generalization and development at the Norwegian Building Research Institute, where the Southampton computer programme was rewritten for a Univac 1107 and then implemented on a Univac 1108. A complete cooling tower analysis which on the Pegasus II in Southampton (1966) would take about 12···14 hours, today (1972) requires about one minute on the 1108.

The present work is based upon the differential equations established by FLÜGGE [1], which the author has arranged in Ch. 2 in a form suitable for a matrix method of numerical integration. The theory of adjoining rings, Ch. 3, and the formulation of boundary conditions, Ch. 4, are given with the objective in mind of achieving generality without being unduly impractical.

The computational scheme outlined in Ch. 5 is a condensed version of a paper previously published by the author [6]. The computational examples of Ch. 6···Ch. 9, with the exception of the cooling towers of Ch. 6, have all been performed with the RSHELL programme, developed at the Norwegian Building Research Institute, and currently running on a Univac 1108 installation in Oslo. These examples were selected in order to present the rather wide field of application for this programme.

2 General equations for thin orthotropic shells of revolution

2.1 *Definitions*

The system of coordinates and displacements of the reference surface of a shell of revolution is shown on Fig. 1. The notation

$$\frac{\partial}{\partial\theta}(\ ) = (\ )', \quad \frac{\partial}{\partial s}(\ ) = (\ )^{\cdot}$$

is used. Note that the independent variable θ is nondimensional while s has dimension of length.

The meridional radius of curvature r_1 is taken as positive when the centre of curvature lies on the normal going from the shell towards the axis.

The relation of the physical shell, which may have ribs and several slab layers, to the reference surface appears in Fig. 2.

Stress resultants and loads are shown in their positive directions in Fig. 3a···b. The indices 1 and 2 refer to directions u and v, respectively.

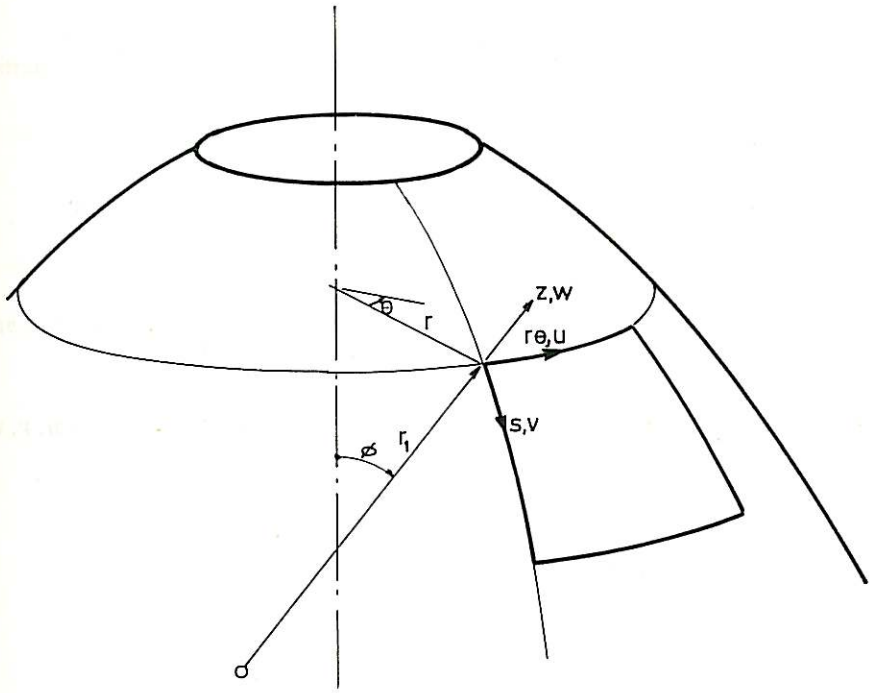

Fig. 1. Coordinates and displacements.

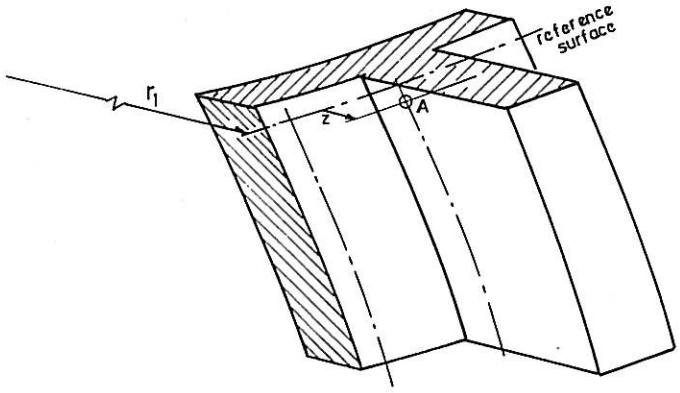

Fig. 2. Physical shell.

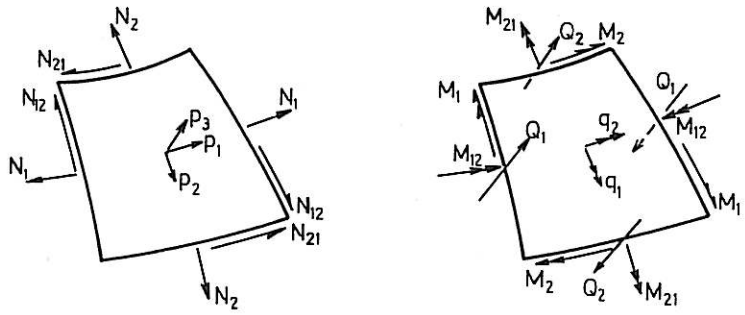

Fig. 3. Stress resultants and loads. a) Extensional group, b) Bending group.

2.2 *Kinematic relations (strain-displacement)*

At a point on the reference surface, the strains for small displacements u, v, w are (see [1], Eq. 2.59)

$$\epsilon_1 = \frac{1}{r}(u' + v\cos\phi + w\sin\phi)$$

$$\epsilon_2 = v^{\cdot} + \frac{w}{r_1} \tag{1}$$

$$\gamma_{12} = u^{\cdot} - u\frac{\cos\phi}{r} + \frac{v'}{r}$$

At a point A located a distance z away from the reference surface the displacements are

$$u_A = u\frac{r + z\sin\phi}{r} - \frac{z}{r}w'$$

$$v_A = v\frac{r_1 + z}{r_1} - zw^{\cdot} \tag{2}$$

$$w_A = w$$

Furthermore

$$\frac{\partial}{\partial s_A} = \frac{r_1}{r_1 + z}\frac{\partial}{\partial s}$$

When $z \ll r, r_1$ we may simplify this to

$$u_A = u - \frac{z}{r}w'$$

$$v_A = v - zw^{\cdot}$$

$$w_A = w \tag{3}$$

$$\frac{\partial}{\partial s_A} = \frac{\partial}{\partial s}$$

The strains ϵ are then

$$\epsilon_1 = \frac{1}{r}(u' + v\cos\phi + w\sin\phi - \frac{z}{r}w'' - w^{\cdot}z\cos\phi)$$

$$\epsilon_2 = v^{\cdot} + \frac{w}{r_1} - zw^{\cdot\cdot} \tag{4}$$

$$\gamma_{12} = u^{\cdot} - \frac{\cos\phi}{r}u + 2z\frac{r^{\cdot}}{r^2}w' - 2\frac{z}{r}w'^{\cdot} + \frac{v'}{r}$$

The displacements can be expressed as a Fourier series in the form

$$u = \sum_{m=0}^{mm} u_m(s)\sin m\theta$$

$$v = \sum_{m=0}^{mm} v_m(s)\cos m\theta \qquad \text{Case I} \tag{5a}$$

$$w = \sum_{m=0}^{mm} w_m(s)\cos m\theta$$

or

$$u = \sum_{m=1}^{mm} u_m(s)\,\cos m\theta$$

$$v = \sum_{m=1}^{mm} v_m(s)\,\sin m\theta \qquad \text{Case II} \tag{5b}$$

$$w = \sum_{m=1}^{mm} w_m(s)\,\sin m\theta$$

As the subsequent development shows, either one of the displacement fields (5a) or (5b) satisfies all differential relationships identically, term by term, in the θ-direction. We may therefore treat each Fourier term independently, writing $u_m(s) = u$ etc. for the sake of brevity.

We now define the dependent function vector

$$\mathbf{F} = \begin{bmatrix} u \\ v \\ w \\ u' \\ v' \\ w' \\ w'' \\ Q_2 \end{bmatrix} \tag{6}$$

and may then write the strain vector

$$\epsilon = \begin{bmatrix} \epsilon_1 \\ \epsilon_2 \\ \gamma_{12} \end{bmatrix} = \begin{bmatrix} \frac{m}{r} & \frac{\cos\phi}{r} & \frac{\sin\phi}{r} & 0 & 0 & 0 & 0 & 0 \\ 0 & 0 & \frac{1}{r_1} & 0 & 1 & 0 & 0 & 0 \\ -\frac{\cos\phi}{r} & -\frac{m}{r} & 0 & 1 & 0 & 0 & 0 & 0 \end{bmatrix} \cdot \mathbf{F}$$

$$+ z \cdot \begin{bmatrix} 0 & 0 & +\frac{m^2}{r^2} & 0 & 0 & \frac{-\cos\phi}{r} & 0 & 0 \\ 0 & 0 & 0 & 0 & 0 & 0 & -1 & 0 \\ 0 & 0 & -2\frac{m\cos\phi}{r^2} & 0 & 0 & 2\frac{m}{r} & 0 & 0 \end{bmatrix} \cdot \mathbf{F} \tag{7}$$

In matrix form

$$\epsilon = (\mathbf{T}_0 + z\mathbf{T}_1)\,\mathbf{F} \tag{8}$$

Eq. (8) represents Case I (5a) when positive m-values are substituted, and Case II (5b) when negative m-values are substituted.

We shall later require the derivatives $\frac{\partial}{\partial s}\mathbf{T}_0$ and $\frac{\partial}{\partial s}\mathbf{T}_1$ and list here the non-zero elements of the matrices:

$$
\begin{aligned}
T_0^{\cdot}(1,1) &= -T_0(3,2) = -\frac{\mathrm{m}\cos\phi}{r^2} \\
T_0^{\cdot}(1,2) &= -T_0^{\cdot}(3,1) = -\frac{r_1\cos^2\phi + r\sin\phi}{r_1 r^2} \\
T_0^{\cdot}(1,3) &= \frac{r\cos\phi - r_1\cos\phi\sin\phi}{r_1 r^2} \\
T_0^{\cdot}(2,3) &= -\frac{r_1^{\cdot}}{r_1^2} \\
T_1^{\cdot}(1,3) &= -\frac{2\mathrm{m}^2\cos\phi}{r^3} \\
T_1^{\cdot}(1,6) &= \frac{r_1\cos^2\phi + r\sin\phi}{r_1 r^2} \\
T_1^{\cdot}(3,3) &= 2\,\mathrm{m}\,\frac{r\sin\phi + 2\,r_1\cos^2\phi}{r_1 r^3} \\
T_1^{\cdot}(3,6) &= \frac{-2\,\mathrm{m}\cos\phi}{r^2}
\end{aligned}
\tag{9}
$$

2.3 *Stress-strain relations*

The shell may consist of a number of orthotropic layers, eventually with ribs in the circumferential and meridional direction.

We have the stress-strain relation within one layer

$$
\begin{bmatrix} \sigma_1 \\ \sigma_2 \\ \tau_{12} \end{bmatrix} = \begin{bmatrix} \dfrac{E_1}{1-\nu_1\nu_2} & E_2\nu_2 & 0 \\ E_1\nu_1 & \dfrac{E_2}{1-\nu_1\nu_2} & 0 \\ 0 & 0 & G \end{bmatrix} \begin{bmatrix} \epsilon_1 - e_1 \\ \epsilon_2 - e_2 \\ \gamma_{12} \end{bmatrix} \tag{10}
$$

$$
\sigma = \mathbf{E}\cdot(\epsilon - \mathbf{e}) \tag{11}
$$

$$
\sigma = \mathbf{E}\ (\mathbf{T}_0 + z\mathbf{T}_1)\,\mathbf{F} - (\mathbf{e}_0 + z\mathbf{e}_1) \tag{12}
$$

where $\mathbf{e}$ represents »initial strains» such as temperature strains, shrinkage etc., $\mathbf{e}_0$ being the initial strains at the reference surface and $\mathbf{e}_1$ the strain gradient across the shell.

2.4 *Stress resultants*

The membrane forces and bending moments in the shell are formed by integrating the stresses over a unit length of the middle surface. Factors of the form $\frac{1}{r_1 + z}$ and $\frac{z}{r_1 + z}$ will appear in the integrals. As is usual in this type of shell theory, we assume $z \ll r_1$, neglecting z compared with r_1 in the denominators. We then have $N_{12} = N_{21}$ and $M_{12} = M_{21}$.

We can then write for the membrane forces

$$\begin{bmatrix} N_1 \\ N_2 \\ N_{12} \end{bmatrix} = \begin{bmatrix} \int_{A_1} & 0 & 0 \\ 0 & \int_{A_2} & 0 \\ 0 & 0 & \int_{A_{12}} \end{bmatrix} \begin{bmatrix} \sigma_1 \\ \sigma_2 \\ \tau_{12} \end{bmatrix} \mathrm{d}A \tag{13}$$

where A_1, A_2 and A_{12} are the sectional areas, per unit length of reference surface, that take meridional, circumferential and shear stress, respectively.

For brevity, we define the operator

$$\mathbf{Z} = \begin{bmatrix} \int_{A_1} & 0 & 0 \\ 0 & \int_{A_2} & 0 \\ 0 & 0 & \int_{A_{12}} \end{bmatrix} \tag{14}$$

and the section rigidity matrix

$$\mathbf{D}_k = \mathbf{Z} \cdot \mathbf{E} z^k \, \mathrm{d}A \qquad k = 0, 1, 2 \tag{15}$$

Using (12) and (13) we can then write for the stress resultants

$$\mathbf{S} = \begin{bmatrix} N_1 \\ N_2 \\ N_{12} \\ M_1 \\ M_2 \\ M_{12} \\ Q_2 \end{bmatrix} = \left[\begin{array}{cc|c} \mathbf{D}_0 & \mathbf{D}_1 & \\ -\mathbf{D}_1 & -\mathbf{D}_2 & 0 \\ \hline 0 & & 1 \end{array}\right] \left[\begin{array}{c} \mathbf{T}_0 \\ \mathbf{T}_1 \\ \hline 1 \end{array}\right] \mathbf{F} - \left[\begin{array}{cc|c} \mathbf{D}_0 & \mathbf{D}_1 & \\ -\mathbf{D}_1 & -\mathbf{D}_2 & 0 \\ \hline 0 & & 1 \end{array}\right] \left[\begin{array}{c} \mathbf{e}_0 \\ \mathbf{e}_1 \\ \hline 0 \end{array}\right] \tag{16}$$

or

$$\mathbf{S} = \mathbf{D} \cdot \mathbf{T} \cdot \mathbf{F} - \mathbf{D} \cdot \mathbf{e} \tag{17}$$

or

$$\mathbf{S} = \mathbf{H} \cdot \mathbf{F} - \mathbf{S}_0 \tag{18}$$

The matrices defined above have the dimensions

$\mathbf{D}_0$ $\mathbf{D}_1$ $\mathbf{D}_2$	3×3
$\mathbf{D}$	7×7
$\mathbf{T}_0$ $\mathbf{T}_1$	3×8
$\mathbf{T}$	7×8
$\mathbf{F}$	8×1
$\mathbf{e}$	7×1

From (17) and (18) it follows that

$$\begin{aligned}\mathbf{S}^{\cdot} &= \mathbf{D}^{\cdot}\mathbf{T}\mathbf{F} + \mathbf{D}\mathbf{T}^{\cdot}\mathbf{F} + \mathbf{D}\mathbf{T}\mathbf{F}^{\cdot} - \mathbf{D}^{\cdot}\mathbf{e} - \mathbf{D}\mathbf{e}^{\cdot} \\ &= \mathbf{H}^{\cdot}\mathbf{F} + \mathbf{H}\mathbf{F}^{\cdot} - \mathbf{S}_0^{\cdot}\end{aligned} \tag{19}$$

2.5 *Force-displacement relations for isotropic shell of variable thickness*

For this case, which is frequently found in practice, we have ((10), (14), (15))

$$\mathbf{D}_k = \int_{-t/2}^{t/2} \begin{bmatrix} z^k & 0 & 0 \\ 0 & z^k & 0 \\ 0 & 0 & z^k \end{bmatrix} \begin{bmatrix} 1 & \nu & 0 \\ \nu & 1 & 0 \\ 0 & 0 & \frac{1+\nu}{2} \end{bmatrix} \frac{E}{1-\nu^2}\, dz \quad k = 0, 1, 2 \tag{20}$$

In performing the integration, we put $\frac{r}{r+z} \approx 1$, hence

$$\mathbf{D}_0 = D \begin{bmatrix} 1 & \nu & 0 \\ \nu & 1 & 0 \\ 0 & 0 & \frac{1-\nu}{2} \end{bmatrix} \tag{21}$$

where $D = \frac{Et}{1-\nu^2}$ is the extensional stiffness of the shell,

$$\begin{aligned}\mathbf{D}_1 &= 0 \\ \mathbf{D}_2 &= K \begin{bmatrix} 1 & \nu & 0 \\ \nu & 1 & 0 \\ 0 & 0 & \frac{1-\nu}{2} \end{bmatrix}\end{aligned} \tag{22}$$

$K = \dfrac{Et^3}{12(1-\nu^2)}$ is the bending stiffness. **D** as defined in (16) is

$$\mathbf{D} = \begin{bmatrix} D & \nu D & 0 & 0 & 0 & 0 & 0 \\ \nu D & D & 0 & 0 & 0 & 0 & 0 \\ 0 & 0 & \frac{1-\nu}{2}D & 0 & 0 & 0 & 0 \\ 0 & 0 & 0 & -K & -\nu K & 0 & 0 \\ 0 & 0 & 0 & -\nu K & -K & 0 & 0 \\ 0 & 0 & 0 & 0 & 0 & -\frac{1-\nu}{2}K & 0 \\ 0 & 0 & 0 & 0 & 0 & 0 & 1 \end{bmatrix} \tag{23}$$

The force-displacement relations (16), using (7) are

$$\mathbf{S} = \begin{bmatrix} N_1 \\ N_2 \\ N_{12} \\ M_1 \\ M_2 \\ M_{12} \\ Q_2 \end{bmatrix} = \begin{bmatrix} D \\ D \\ \frac{1-\nu}{2}D \\ K \\ K \\ (1-\nu)K \\ 1 \end{bmatrix}_{\text{Diag}} \times \begin{bmatrix} \frac{\mathrm{m}}{r} & \frac{\cos\phi}{r} & \frac{\sin\phi}{r}+\frac{\nu}{r_1} & 0 & \nu & 0 & 0 & 0 \\ \frac{\nu\mathrm{m}}{r} & \frac{\nu\cos\phi}{r} & \frac{\nu\sin\phi}{r}+\frac{1}{r_1} & 0 & 1 & 0 & 0 & 0 \\ \frac{\cos\phi}{r} & -\frac{\mathrm{m}}{r} & 0 & 1 & 0 & 0 & 0 & 0 \\ 0 & 0 & -\frac{\mathrm{m}^2}{r^2} & 0 & 0 & \frac{\cos\phi}{r} & \nu & 0 \\ 0 & 0 & -\frac{\nu\mathrm{m}^2}{r^2} & 0 & 0 & \frac{\nu\cos\phi}{r} & 1 & 0 \\ 0 & 0 & \frac{\mathrm{m}\cos\phi}{r^2} & 0 & 0 & -\frac{\mathrm{m}}{r} & 0 & 0 \\ 0 & 0 & 0 & 0 & 0 & 0 & 0 & 1 \end{bmatrix} \begin{bmatrix} u \\ v \\ w \\ u' \\ v' \\ w' \\ w'' \\ Q_2 \end{bmatrix} - \begin{bmatrix} (1+\nu)De^\circ \\ (1+\nu)De^\circ \\ 0 \\ -(1+\nu)K\bar{e} \\ -(1+\nu)K\bar{e} \\ 0 \\ 0 \end{bmatrix} \tag{24}$$

where e° is the uniform initial strain (e.g. from temperature or shrinkage) and $\bar{e}$ is the strain gradient across the shell thickness.

Eq. (24) can be written in the form (18)

$$\mathbf{S} = \psi\mathbf{h}\mathbf{F} - \mathbf{S}_0 = \mathbf{H}\mathbf{F} - \mathbf{S}_0 \tag{25}$$

Further

$$\mathbf{S}^\cdot = \psi^\cdot\mathbf{h}\mathbf{F} + \psi\mathbf{h}^\cdot\mathbf{F} + \psi\mathbf{h}\mathbf{F}^\cdot - \mathbf{S}_0^\cdot$$

$$\mathbf{S}^\cdot = \mathbf{H}^\cdot\mathbf{F} + \mathbf{H}\mathbf{F}^\cdot - \mathbf{S}_0^\cdot$$

where

$$\psi^\cdot = \left[D^\cdot D^\cdot \frac{1-\nu}{2}D^\cdot K^\cdot K^\cdot (1-\nu)K^\cdot\ 0\right]\text{diag}$$

and $\mathbf{h}^{\cdot}$ has the non-zero elements

$$h^{\cdot}(1,1) = -h^{\cdot}(3,2) = -h^{\cdot}(6,6) = -\frac{\mathrm{m}\cos\phi}{r^2}$$

$$h^{\cdot}(2,1) = \nu \cdot h^{\cdot}(1,1)$$

$$h^{\cdot}(1,2) = -h^{\cdot}(3,1) = h^{\cdot}(4,6) = -\frac{r_1\cos^2\phi + r\sin\phi}{r_1 r^2}$$

(23)

$$h^{\cdot}(2,2) = h(5,6) = \nu \cdot h^{\cdot}(1,2)$$

$$h^{\cdot}(1,3) = \frac{r\cos\phi - r_1\cos\phi\sin\phi}{r_1 r^2} - \nu\frac{\dot{r_1}}{r_1^2} \qquad (26)$$

$$h^{\cdot}(2,3) = \nu\frac{r\cos\phi - r_1\cos\phi\sin\phi}{r_1 r^2} - \frac{\dot{r_1}}{r_1^2}$$

$$h^{\cdot}(4,3) = \frac{2\,\mathrm{m}^2\cos\phi}{r^3}$$

$$h^{\cdot}(5,3) = \nu \cdot h^{\cdot}(4,3)$$

$$h^{\cdot}(6,3) = -\,\mathrm{m}\,\frac{r\sin\phi + 2r_1\cos^2\phi}{r_1 r^3}$$

2.6 *Equilibrium equations*

(24)

FLÜGGE [1] has established five equations of equilibrium for shells of revolution. These equations in our notation and with moment loads q_1 and q_2 (Fig. 3) included are

$$\begin{aligned}
&r_1 N_1' + r_1 N_{12}\cos\phi + (rN_{12})^{\circ} - r_1 Q_1\sin\phi = -rr_1 p_1\\
&-r_1 N_1\cos\phi + (rN_2)^{\circ} + r_1 N_{12}' - rQ_2 = -rr_1 p_2\\
&r_1 N_1\sin\phi + rN_2 + r_1 Q_1' + (rQ_2)^{\circ} = rr_1 p_3 \qquad (27a\cdots e)\\
&-r_1 M_1\cos\phi + (rM_2)^{\circ} + r_1 M_{12}' - rr_1 Q_2 = rr_1 q_2\\
&-rM_1' + r_1 M_{12}\cos\phi + (rM_{12})^{\circ} - rr_1 Q_1 = -rr_1 q_1
\end{aligned}$$

the

where

25)

$$(\ )^{\circ} = \frac{\partial}{\partial\phi}(\ ),\quad (\ )' = \frac{\partial}{\partial\theta}(\ )$$

also

$$r^{\circ} = r_1\cos\phi$$

As can be readily verified, the assumed displacement field (5a), resp. (5b) implies stress resultants and loads of the form

(5a) – Case I

$$\begin{bmatrix} N_1 \\ N_2 \\ N_{12} \\ M_1 \\ M_2 \\ M_{12} \\ Q_2 \end{bmatrix} (\theta, s) = \sum_{m=0}^{mm} \begin{bmatrix} \cos m\theta & 0 & 0 & 0 & 0 & 0 & 0 \\ 0 & \cos m\theta & 0 & 0 & 0 & 0 & 0 \\ 0 & 0 & \sin m\theta & 0 & 0 & 0 & 0 \\ 0 & 0 & 0 & \cos m\theta & 0 & 0 & 0 \\ 0 & 0 & 0 & 0 & \cos m\theta & 0 & 0 \\ 0 & 0 & 0 & 0 & 0 & \sin m\theta & 0 \\ 0 & 0 & 0 & 0 & 0 & 0 & \cos m\theta \end{bmatrix} \begin{bmatrix} N_1 \\ N_2 \\ N_{12} \\ M_1 \\ M_2 \\ M_{12} \\ Q_2 \end{bmatrix} (s) \tag{28}$$

or

$$\mathbf{S}(\theta, s) = \sum_{m=0}^{mm} \mathbf{X}_s(\theta)\, \mathbf{S}(s) \tag{29}$$

and

$$\begin{bmatrix} p_1 \\ p_2 \\ p_3 \\ q_1 \\ q_2 \end{bmatrix} (\theta, s) = \sum_{m=0}^{mm} \begin{bmatrix} \sin m\theta & 0 & 0 & 0 & 0 \\ 0 & \cos m\theta & 0 & 0 & 0 \\ 0 & 0 & \cos m\theta & 0 & 0 \\ 0 & 0 & 0 & \sin m\theta & 0 \\ 0 & 0 & 0 & 0 & \cos m\theta \end{bmatrix} \begin{bmatrix} p_1 \\ p_2 \\ p_3 \\ q_1 \\ q_2 \end{bmatrix} (s) \tag{30}$$

or

$$\mathbf{P}(\theta, s) = \sum_{m=0}^{mm} \mathbf{X}_p(\theta)\, \mathbf{P}(s) \tag{31}$$

For the antimetric case (5b) we have

$$\mathbf{S}^{\star}(\theta, s) = \sum_{m=1}^{mm} \mathbf{X}_s^{\star}(\theta)\, \mathbf{S}(s) \tag{32}$$

$$\mathbf{P}^{\star}(\theta, s) = \sum_{m=1}^{mm} \mathbf{X}_p^{\star}(\theta)\, \mathbf{P}(s) \tag{33}$$

where $\mathbf{X}_s^{\star}$ and $\mathbf{X}_p^{\star}$ are the complements of $\mathbf{X}_s$ and $\mathbf{X}_p$, being obtained by replacing $\sin m\theta$ by $\cos m\theta$ and vice versa.

It can be seen by inspection that the above expansions (29), (31) and (32)···(33) satisfy Eqs. (27) term by term, in θ, so that the partial differential Equations (27) are reduced to a set of ordinary differential equations.

We now use Eq. (27d) to eliminate Q_1 and make the change of coordinate from ϕ to s

$$( )^{\circ} = \frac{\partial}{\partial \phi}( ) = r_1 \frac{\partial}{\partial s}( ) = r_1( )^{\cdot} \tag{34}$$

The four remaining equilibrium equations are then

$$\begin{bmatrix} -\mathrm{m} & 0 & 2\cos\phi & \mathrm{m}\dfrac{\sin\phi}{r} & 0 & -\dfrac{2}{r}\sin\phi\cos\phi & 0 \\ -\cos\phi & \cos\phi & \mathrm{m} & 0 & 0 & 0 & -\dfrac{r}{r_1} \\ \sin\phi & \dfrac{r}{r_1} & 0 & -\dfrac{\mathrm{m}^2}{r} & 0 & 2\mathrm{m}\dfrac{\cos\phi}{r} & \cos\phi \\ 0 & 0 & 0 & -\dfrac{\cos\phi}{r} & \dfrac{\cos\phi}{r} & \dfrac{\mathrm{m}}{r} & -1 \end{bmatrix} \begin{bmatrix} N_1 \\ N_2 \\ N_{12} \\ M_1 \\ M_2 \\ M_{12} \\ Q_2 \end{bmatrix}$$

$$+ \begin{bmatrix} 0 & 0 & r & 0 & 0 & -\sin\phi & 0 \\ 0 & r & 0 & 0 & 0 & 0 & 0 \\ 0 & 0 & 0 & 0 & 0 & \mathrm{m} & r \\ 0 & 0 & 0 & 0 & 1 & 0 & 0 \end{bmatrix} \begin{bmatrix} N_1 \\ N_2 \\ N_{12} \\ M_1 \\ M_2 \\ M_{12} \\ Q_2 \end{bmatrix}^{\cdot} = \begin{bmatrix} -rp_1 + q_1\sin\phi \\ -rp_2 \\ rp_3 - \mathrm{m}q_1 \\ q_2 \end{bmatrix} \tag{35}$$

in matrix notation

$$\mathbf{L}_0\mathbf{S} + \mathbf{L}_1\mathbf{S}^{\cdot} = \mathbf{Q} \tag{36}$$

using (18) and (19)

$$\mathbf{L}_0(\mathbf{HF} - \mathbf{S}_0) + \mathbf{L}_1(\mathbf{H}^{\cdot}\mathbf{F} + \mathbf{HF}^{\cdot} - \mathbf{S}_0^{\cdot}) = \mathbf{Q}$$

$$\mathbf{L}_1\mathbf{HF}^{\cdot} = -(\mathbf{L}_0\mathbf{H} + \mathbf{L}_1\mathbf{H}^{\cdot})\mathbf{F} + (\mathbf{Q} + \mathbf{L}_0\mathbf{S}_0 + \mathbf{L}_1\mathbf{S}_0^{\cdot}) \tag{37}$$

or

$$\mathbf{C}'\mathbf{F}^{\cdot} = \mathbf{A}'\mathbf{F} + \mathbf{B}' \tag{38}$$

By definition of the function vector $\mathbf{F}$ we have four further equations

$$\begin{bmatrix} 1 & 0 & 0 & 0 & 0 & 0 & 0 & 0 \\ 0 & 1 & 0 & 0 & 0 & 0 & 0 & 0 \\ 0 & 0 & 1 & 0 & 0 & 0 & 0 & 0 \\ 0 & 0 & 0 & 0 & 0 & 1 & 0 & 0 \end{bmatrix} \begin{bmatrix} u \\ v \\ w \\ u^{\cdot} \\ v^{\cdot} \\ w^{\cdot} \\ w^{\cdot\cdot} \\ Q_2 \end{bmatrix}^{\cdot} = \begin{bmatrix} 0 & 0 & 0 & 1 & 0 & 0 & 0 & 0 \\ 0 & 0 & 0 & 0 & 1 & 0 & 0 & 0 \\ 0 & 0 & 0 & 0 & 0 & 1 & 0 & 0 \\ 0 & 0 & 0 & 0 & 0 & 0 & 1 & 0 \end{bmatrix} \begin{bmatrix} u \\ v \\ w \\ u^{\cdot} \\ v^{\cdot} \\ w^{\cdot} \\ w^{\cdot\cdot} \\ Q_2 \end{bmatrix}$$

or

$$\mathbf{C}''\mathbf{F}^{\cdot} = \mathbf{A}''\mathbf{F} + \mathbf{O} \tag{39}$$

Equations (38) and (39) form a set of eight simultaneous, linear differential equations

$$\left[\frac{\mathbf{C}'}{\mathbf{C}''}\right]\mathbf{F}^{\cdot} = \left[\frac{\mathbf{A}'}{\mathbf{A}''}\right]\mathbf{F} + \left[\frac{\mathbf{B}'}{\mathbf{O}}\right] \tag{40}$$

which by inversion is transformed to

$$\mathbf{F}^{\cdot} = \mathbf{A}\mathbf{F} + \mathbf{B} \tag{41}$$

where **A** is (8 × 8) and **F** (8 × 1).

Eqs. (41) contain the kinematic relations, the stress-strain relations and the equilibrium equations for a shell of revolution of arbitrary meridional form and with arbitrary loading, including initial (temperature) strains.

2.7 *Axisymmetric case*

For this case (m = 0) the displacement u and its derivatives are zero. The system (41) is then reduced to a system of 6 simultaneous equations, i.e. the 1. and 4. of the equations (41) become identities. In a computer programme this situation can be conveniently handled by compressing the **A**-matrix to a 6 × 6 matrix by eliminating the 1. and 4. rows and columns, and the 1. and 4. elements of **B**, for example by pre- and postmultiplying by suitable elimination matrices.

3 Equations for elastic rings

The load-stress-displacement relations for elastic rings will be developed below. The treatment is restricted to rings of such cross-section that warping does not take place or may be neglected and consequently, that the torsional resistance is due to St. Venant torsion of a solid section or of individual parts of an open, thin-walled cross section, or a shear flow around a tubular cross section. Such forms are shown in Fig. 4a···f.

This restriction does not, in fact, impose excessive limitations on the types of stiffening ring shapes that can be treated, as the basic ring forms in Fig. 4a···e can be combined with elements, considered as part of the shell proper, to provide shapes in which warping does take place and where stiffness and stresses due to warping are not neglected. Such composite sections are shown in Fig. 4g···h.

3.1 *Ring displacements – degrees of freedom*

The ring is considered to be a curved beam of generally asymmetric cross section, i.e. the shear centre generally does not coincide with the centre of gravity. The ring geometry and coordinates are shown in Fig. 5 where the centre of gravity is denoted with G and the shear centre with S. The external loads and stress resultants are shown in Figs. 6 and 7.

For a particular Fourier term m, the ring has four independent degrees of freedom, viz. translations u_1, u_2, u_3 of G in x, y, z direction and a rotation u_4 about the shear centre.

The displacement vector has the form

$$\mathbf{u} = \begin{bmatrix} u_1 \sin m\theta \\ u_2 \cos m\theta \\ u_3 \cos m\theta \\ u_4 \cos m\theta \end{bmatrix} = \begin{bmatrix} u_1 \\ u_2 \\ u_3 \\ u_4 \end{bmatrix} \tag{42}$$

for a term of Case I and has the complementary form for a term of Case II. Only the Case I terms will be considered here; the Case II terms can be considered merely by substituting negative m-values in the expressions developed.

The rotations u_5 and u_6 about axes 2 and 3 respectively, merely represent variation along the ring of u_3 and u_2

$$\begin{aligned} u_5 &= \frac{\partial}{R\partial\theta} u_3 = -\frac{m}{R} u_3 \sin m\theta \\ u_6 &= -\frac{\partial}{R\partial\theta} u_2 = \frac{m}{R} u_2 \sin m\theta \end{aligned} \tag{43}$$

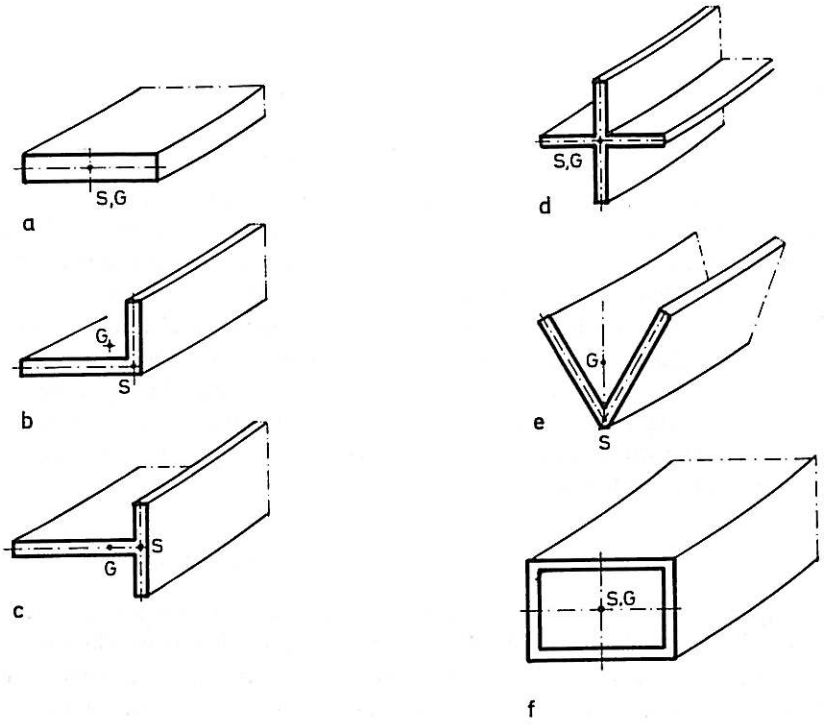

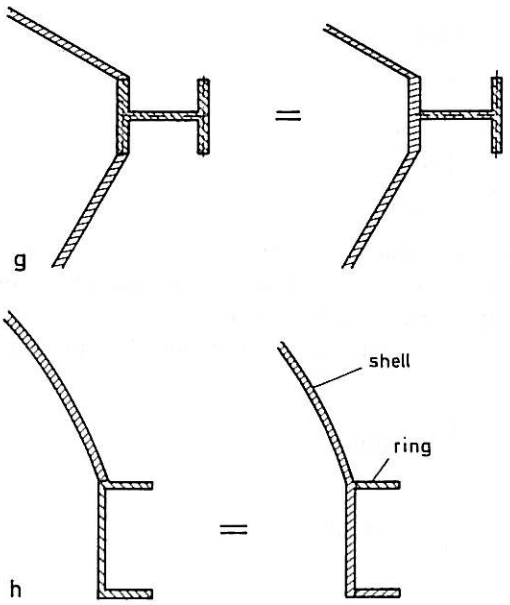

S = shear centre
G = centre of gravity

Fig. 4. Ring forms.

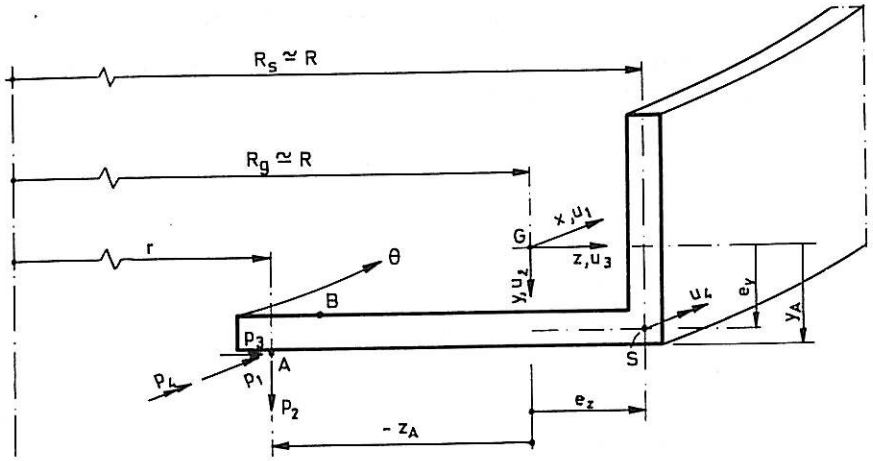

Fig. 5. Ring geometry.

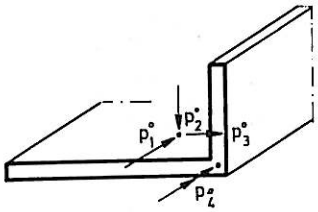

Fig. 6. External loads.

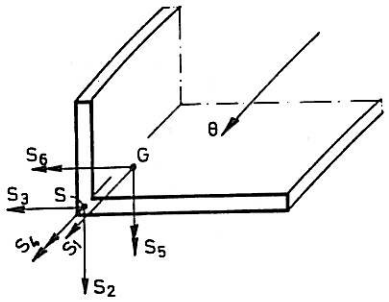

Fig. 7. Stress resultants.

so that the augmented displacement vector $\mathbf{u}^*$ is

$$\mathbf{u}^* = \begin{bmatrix} u_1 \\ u_2 \\ u_3 \\ u_4 \\ u_5 \\ u_6 \end{bmatrix} = \begin{bmatrix} 1 & 0 & 0 & 0 \\ 0 & 1 & 0 & 0 \\ 0 & 0 & 1 & 0 \\ 0 & 0 & 0 & 1 \\ 0 & 0 & -\frac{m}{R} & 0 \\ 0 & \frac{m}{R} & 0 & 0 \end{bmatrix} \begin{bmatrix} u_1 \\ u_2 \\ u_3 \\ u_4 \end{bmatrix} = \mathbf{C} \cdot \mathbf{u} \tag{44}$$

3.2 *Ring displacements in terms of shell actions*

The kinematic relations between the shell displacements at point A and the ring displacements as defined in Sec. 3.1 are (see Fig. 8)

$$u_1 = \frac{R}{r}\,u - \frac{\mathrm{m}}{r}\,((z_\mathrm{A}\cos\phi + y_\mathrm{A}\sin\phi)\,v + (z_\mathrm{A}\sin\phi - y_\mathrm{A}\cos\phi)\,w)$$

$$u_2 = v\sin\phi - w\cos\phi + z_\mathrm{A}\cdot w'$$

$$u_3 = v\cos\phi + w\sin\phi - y_\mathrm{A}\cdot w'$$

$$u_4 = -w'$$

Let

$$z_\mathrm{A}\cos\phi + y_\mathrm{A}\sin\phi = e_1$$

$$z_\mathrm{A}\sin\phi - y_\mathrm{A}\cos\phi = e_2$$

In matrix form

$$\mathbf{u} = \begin{bmatrix} u_1 \\ u_2 \\ u_3 \\ u_4 \end{bmatrix} = \begin{bmatrix} \frac{R}{r} & -\frac{\mathrm{m}e_1}{r} & -\frac{\mathrm{m}e_2}{r} & 0 & 0 & 0 & 0 & 0 \\ 0 & \sin\phi & -\cos\phi & 0 & 0 & z & 0 & 0 \\ 0 & \cos\phi & \sin\phi & 0 & 0 & -y & 0 & 0 \\ 0 & 0 & 0 & 0 & 0 & -1 & 0 & 0 \end{bmatrix}_\mathrm{A} \begin{bmatrix} u \\ v \\ w \\ u' \\ v' \\ w' \\ w'' \\ Q_2 \end{bmatrix}_\mathrm{A}$$

or

$$\mathbf{u} = \mathbf{T}_\mathrm{A}\mathbf{F}_\mathrm{A} \tag{45}$$

For the other shell, which is joined to the ring at point B, we have similarly

$$\mathbf{u} = \mathbf{T}_\mathrm{B}\mathbf{F}_\mathrm{B} \tag{46}$$

and kinematic compatibility between the two shells joining the ring is therefore given by

$$\mathbf{T}_\mathrm{A}\mathbf{F}_\mathrm{A} = \mathbf{T}_\mathrm{B}\mathbf{F}_\mathrm{B} \tag{47}$$

3.3 *Strains and strain energy*

For Case I, the stress resultants as shown in Fig. 7, have the form

$$\begin{array}{ll} S_1\cos\mathrm{m}\theta & S_4\sin\mathrm{m}\theta \\ S_2\sin\mathrm{m}\theta & S_5\cos\mathrm{m}\theta \\ S_3\sin\mathrm{m}\theta & S_6\cos\mathrm{m}\theta \end{array}$$

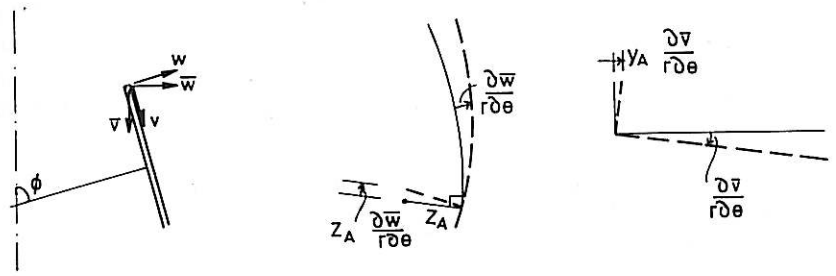

Fig. 8. The shell displacements at point A and the ring displacements.

The generalized strains are

$$\epsilon_1 = \frac{1}{R} u_1' + \frac{1}{R} u_3 = \frac{\mathrm{m}}{R} u_1 + \frac{1}{R} u_3$$

$$\epsilon_2 = \epsilon_3 = 0$$

$$\epsilon_4 = \frac{1}{R} u_4' + \frac{1}{R} u_6 = -\frac{\mathrm{m}}{R} u_4 + \frac{\mathrm{m}}{R^2} u_2$$

$$\epsilon_5 = \frac{1}{R} u_5' = -\frac{\mathrm{m}^2}{R^2} u_3$$

$$\epsilon_6 = \frac{1}{R} u_6' - \frac{1}{R} u_4 = \frac{\mathrm{m}^2}{R^2} u_2 - \frac{1}{R} u_4$$

The vector of the four non-zero generalized strains is then

$$\epsilon = \begin{bmatrix} \epsilon_1 \\ \epsilon_4 \\ \epsilon_5 \\ \epsilon_6 \end{bmatrix} = \begin{bmatrix} \frac{\mathrm{m}}{R} & 0 & \frac{1}{R} & 0 \\ 0 & \frac{\mathrm{m}}{R^2} & 0 & -\frac{\mathrm{m}}{R} \\ 0 & 0 & -\frac{\mathrm{m}^2}{R^2} & 0 \\ 0 & \frac{\mathrm{m}^2}{R^2} & 0 & -\frac{1}{R} \end{bmatrix} \begin{bmatrix} u_1 \\ u_2 \\ u_3 \\ u_4 \end{bmatrix} \tag{48}$$

$$\epsilon = \mathbf{V} \cdot \mathbf{u} \tag{49}$$

The stress resultants in the ring are

$$\begin{bmatrix} S_1 \\ S_4 \\ S_5 \\ S_6 \end{bmatrix} = \begin{bmatrix} EA & 0 & 0 & 0 \\ 0 & GJ & 0 & 0 \\ 0 & 0 & EI_2 & 0 \\ 0 & 0 & 0 & EI_3 \end{bmatrix} \begin{bmatrix} \epsilon_1 \\ \epsilon_4 \\ \epsilon_5 \\ \epsilon_6 \end{bmatrix} \tag{50}$$

or

$$\mathbf{S} = \mathbf{K} \cdot \epsilon = \mathbf{K} \cdot \mathbf{V} \cdot \mathbf{u} \tag{51}$$

We may now express the strain energy of the ring in terms of the displacements:

$$U = \frac{1}{2} \int_0^{2\pi} \{\mathbf{S}\}\, \epsilon R \mathrm{d}\theta = \frac{\pi R}{2}\, \mathbf{u}^{\mathrm{T}} \mathbf{V}^{\mathrm{T}} \mathbf{K} \mathbf{V} \mathbf{u} \tag{52}$$

3.4 *Potential energy of external forces on ring*

Displacements of point A (Fig. 5) are

$$u_1(\mathrm{A}) = \frac{r}{R} u_1 + y_{\mathrm{A}} \cdot u_6 - z_{\mathrm{A}} u_5 = \frac{r}{R} u_1 + y_{\mathrm{A}} \frac{\mathrm{m}}{R} u_2 + z_{\mathrm{A}} \frac{\mathrm{m}}{R} u_3$$

$$u_2(\mathrm{A}) = u_2 - (e_z - z_{\mathrm{A}})\, u_4$$

$$u_3(\mathrm{A}) = u_3 - (y_{\mathrm{A}} - e_{\mathrm{y}})\, u_4$$

$$u_4(\mathrm{A}) = u_4$$

$$u_5(\mathrm{A}) = -\frac{\mathrm{m}}{r} u_3(\mathrm{A}) = -\frac{\mathrm{m}}{R} u_3 + \frac{\mathrm{m}}{R} (y_{\mathrm{A}} - e_{\mathrm{y}})\, u_4$$

$$u_6(\mathrm{A}) = \frac{\mathrm{m}}{R} u_2(\mathrm{A}) = \frac{\mathrm{m}}{R} u_2 - \frac{\mathrm{m}}{R} (e_z - z_{\mathrm{A}})\, u_4$$

$$\mathbf{u}_{\mathrm{A}} = \mathbf{C}_{\mathrm{A}} \mathbf{u} \tag{53}$$

External forces at point A are the forces from the shell. These are decomposed and combined with forces in the direction of $u_1 \cdots u_4$ at point A.

$$p_1 = (N_{12} - \frac{1}{r} M_{12} \sin\phi)\, r \sin\mathrm{m}\theta$$

$$p_2 = (N_2 \sin\phi + (Q_2 + \frac{\mathrm{m}}{r} M_{12}) \cos\phi) \cos\mathrm{m}\theta$$

$$p_3 = (N_2 \cos\phi - (Q_2 + \frac{\mathrm{m}}{r} M_{12}) \sin\phi) \cos\mathrm{m}\theta$$

$$p_4 = -M_2 \cos\mathrm{m}\theta$$

$$\mathbf{p}_{\mathrm{A}} = \mathbf{D}_{\mathrm{A}} \mathbf{S}_{\mathrm{A}} \tag{54}$$

The loads at point B where the second shell segment joins the ring, are

$$\mathbf{p}_{\mathrm{B}} = -\mathbf{D}_{\mathrm{B}} \mathbf{S}_{\mathrm{B}} \tag{55}$$

Finally, there may be a set of external loads $p_1^\circ \cdots p_4^\circ$ acting on the ring as shown in Fig. 6.

During displacement and deformation of the ring, the change in potential energy of all these forces acting on the ring is

$$\Omega = -\int_0^{2\pi} \{(\mathbf{u}^T \mathbf{p} r)_A - (\mathbf{u}^T \mathbf{p} r)_B + (\mathbf{u}^T \mathbf{p} r)_0\} f(\theta)\, d\theta \tag{56}$$

where

$$f(\theta) = \begin{cases} \cos^2 m\theta \\ \sin^2 m\theta \end{cases} \quad \text{and} \quad \int_0^{2\pi} f(\theta)\, d\theta = \pi$$

Substituting (54) and (55) into (56) and rearranging, we get

$$\Omega = -\pi \mathbf{u}^T ((r\mathbf{C}^T \mathbf{D} \mathbf{H} \mathbf{F})_A - (r\mathbf{C}^T \mathbf{D} \mathbf{H} \mathbf{F})_B + (R\mathbf{p})_0) \tag{57}$$

3.5 *Minimization of potential energy of ring*

The kinematic relations (47) are four equations connecting the actions at point B with the actions at point A. The remaining four equations are found by considering the elastic law of the ring, i.e. the relations between forces acting on the ring and deformations of the ring. These equations are readily established by using the principle of minimum potential energy.

The total potential energy W of the ring is the sum of the strain energy and the energy of the applied loads, as given by (52) and (57) respectively:

$$W = U + \Omega \tag{58}$$

The principle of minimum potential energy requires that the generalized displacements $u_1 \cdots u_4$ be such that $\frac{\partial}{\partial u_1} W = 0$, $\frac{\partial}{\partial u_2} W = 0$ etc.

Using (52) and (57) we notice that

$$\frac{\partial}{\partial u_i} U = \frac{\pi R}{2} \frac{\partial}{\partial u_i} \mathbf{u}^T \mathbf{V}^T \mathbf{K} \mathbf{V} \mathbf{u} = \frac{\pi R}{2} \left\{ \frac{\partial \mathbf{u}^T}{\partial u_i} \mathbf{V}^T \mathbf{K} \mathbf{V} \mathbf{u} + \mathbf{u}^T \mathbf{V}^T \mathbf{K} \mathbf{V} \frac{\partial \mathbf{u}}{\partial u_i} \right\} = \pi R [\mathbf{V}^T \mathbf{K} \mathbf{V}] \mathbf{u}$$
$$i = 1, \ldots, 4 \tag{59}$$

because the expression $\frac{\partial}{\partial u_i} U$ is a scalar and the second term in the second form therefore can be transposed and added to the first term ($\mathbf{K}$ is symmetric). Furthermore we note that

$$\frac{\partial \mathbf{u}^T}{\partial u_1} = \{1 \quad 0 \quad 0 \quad 0\} \quad \text{etc.}$$

Differentiating (57) we then get

$$R[\mathbf{V}^T \mathbf{K} \mathbf{V}]\, \mathbf{u} - (r[\mathbf{C}^T \mathbf{D} \mathbf{H}]_A \mathbf{F}_A - r[\mathbf{C}^T \mathbf{D} \mathbf{H}]_B \mathbf{F}_B + R\mathbf{p}_0) = 0$$

or

$$\mathbf{Qu} = \mathbf{Z_A F_A} - \mathbf{Z_B F_B} + \mathbf{P} \tag{60}$$

Using either (45) or (46) we can eliminate **u** from (60). Using (45) and rearranging we get

$$\mathbf{Z_B F_B} = (\mathbf{Z_A} - \mathbf{Q T_A})\,\mathbf{F_A} + \mathbf{P} \tag{61}$$

Combining (47) and (61) we have a system of 8 equations between the shell actions at points A and B, i.e. on either side of the ring:

$$\begin{pmatrix} \mathbf{T_B} \\ \hline \mathbf{Z_B} \end{pmatrix} \mathbf{F_B} = \begin{pmatrix} \mathbf{T_A} \\ \hline \mathbf{Z_A} - \mathbf{Q T_A} \end{pmatrix} \mathbf{F_A} + \begin{pmatrix} \mathbf{0} \\ \hline \mathbf{P} \end{pmatrix} \tag{62}$$

Inverting, we get the system in the form

$$\mathbf{F_B} = \mathbf{G_R F_A} + \mathbf{L_R} \tag{63}$$

when $\mathbf{G_R}$ is the transfer matrix covering the ring between A and B, and **L** the load vector.

For the axisymmetric case (m = 0) u and u' are zero and the 1. and 4. rows and columns of (62) must be eliminated before inverting, leaving a system of 6 equations (see 2.6).

3.6 *Stress resultants in ring*

Knowing the ring displacement vector **u**, the four stress resultants $S = \{S_1\ S_4\ S_5\ S_6\}$ can be found from (51)

$$\mathbf{S} = \mathbf{K V u}$$

The two transverse shears S_2 and S_3 are given by

$$S_3 = \frac{\partial}{R\partial\theta} S_5 = -\frac{\mathrm{m}}{R} S_5$$

$$S_2 = \frac{\partial}{R\partial\theta} S_6 = -\frac{\mathrm{m}}{R} S_6 \tag{64}$$

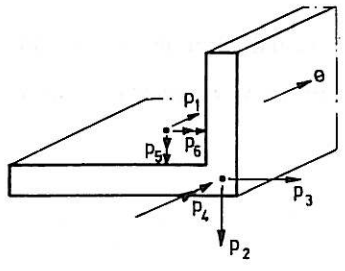

Fig. 9. Loads acting upon the ring.

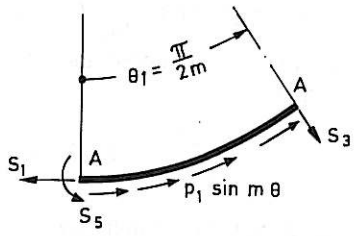

Fig. 10. The tangential load p_1 on a section of the ring.

It is often useful, however, to be able to compute the stress resultants directly from the loads acting on the ring, based upon internal equilibrium in the ring. These relations will be given below.

We assume that the ring is acted upon by loads $p_1 \cdots p_6$ acting partly in G and partly in S as shown in Fig. 9.

Consider first the tangential load p_1 on a section of the ring going from $\theta_0 = 0$ to $\theta_1 = \pi/2m$ (Fig. 10). Only those stress resultants in the ring plane that are shown have values $\neq 0$.

For the equilibrium in the direction $\theta = 0$, we have

$$S_3 \cos\theta_1 = \int_0^{\theta_1} p_1 \sin m\theta \, \sin\theta \, R d\theta = \frac{R}{m^2 - 1} \cos\theta_1 \cdot p_1$$

$$S_3 = \frac{R}{m^2 - 1} p_1 \sin m\theta \tag{65}$$

For the moment equilibrium about A, we have

$$S_3 R \sin\theta_1 - \int_0^{\theta_1} p_1 \sin m\theta \, (1 - \cos\theta) R^2 d\theta - S_5 = 0$$

giving

$$S_5 = \frac{R^2}{m(m^2 - 1)} p_1 \cos m\theta \tag{66}$$

By considering the horizontal equilibrium we obtain

$$S_1 = \frac{m}{m^2 - 1} R p_1 \cos m\theta \tag{67}$$

Treating the other loads in a similar manner, we obtain the complete relationship between ring loads and stress resultants:

$$\begin{bmatrix} S_1 \\ S_2 \\ S_3 \\ S_4 \\ S_5 \\ S_6 \end{bmatrix} = \begin{bmatrix} R\frac{m}{m^2-1} & 0 & \frac{-R}{m^2-1} & 0 & 0 & 0 \\ 0 & -\frac{R}{m} & 0 & 0 & 0 & 0 \\ \frac{R}{m^2-1} & 0 & -R\frac{m}{m^2-1} & 0 & 0 & 0 \\ 0 & \frac{-R^2}{m(m^2-1)} & 0 & -R\frac{m}{m^2-1} & 0 & \frac{-R}{m^2-1} \\ R^2\frac{1}{m(m^2-1)} & 0 & -\frac{R^2}{m^2-1} & 0 & \frac{R}{m} & 0 \\ 0 & \frac{R^2}{m^2-1} & 0 & \frac{R}{m^2-1} & 0 & R\frac{m}{m^2-1} \end{bmatrix} \begin{bmatrix} p_1 \\ p_2 \\ p_3 \\ p_4 \\ p_5 \\ p_6 \end{bmatrix}_0$$

$$\mathbf{S} = \psi \cdot \mathbf{p}^* \tag{68}$$

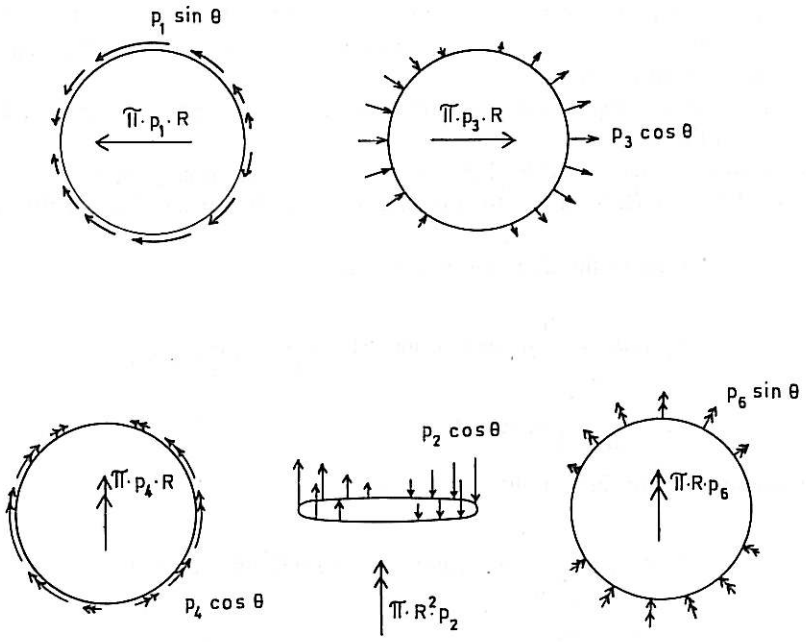

Fig. 11. Ring equilibrium for m = 1.

The above relations do not hold for the case m = 1. This is so because in that case the loads on the ring cannot be independent. In order to ensure the total equilibrium of the ring, the following relations must be fulfilled (see Fig. 11),

$$\begin{aligned} p_1 - p_3 &= 0 \\ Rp_2 + p_4 + p_6 &= 0 \end{aligned} \tag{69}$$

Indeed, if the relations (69) are introduced in (68), the expressions for S_1, S_3, S_4, S_5, S_6 become indefinite, indicating that we are dealing with a hyperstatic problem, and the stress resultants must be found from (51).

In order to use the relation (68), the loads p_i must act as shown in Fig. 9. Loads acting at an arbitrary point A with radius r are transformed to loads acting as shown in Fig. 9 by the following relation

$$\mathbf{p}^* = \begin{bmatrix} p_1 \\ p_2 \\ p_3 \\ p_4 \\ p_5 \\ p_6 \end{bmatrix} = \frac{r}{R} \begin{bmatrix} 1 & 0 & 0 & 0 \\ 0 & 1 & 0 & 0 \\ 0 & 0 & 1 & 0 \\ 0 & -(e_z - z_A) & -(y_A - e_y) & 1 \\ -z_A & 0 & 0 & 0 \\ y_A & 0 & 0 & 0 \end{bmatrix} \begin{bmatrix} p_1 \\ p_2 \\ p_3 \\ p_4 \end{bmatrix}_A \tag{70}$$

For the case m = 0 we must have

$$p_1 = p_2 = p_5 = p_6 \equiv 0 \tag{71}$$

The relations (68) then reduce to

$$\begin{aligned} S_1 &= R \cdot p_3 \\ S_2 &= S_3 = S_4 = 0 \\ S_5 &= R^2 p_3 \\ S_6 &= -R p_4 \end{aligned} \tag{72}$$

4 The formulation of boundary conditions

4.1 *General*

As shown in Ch. 2, the relations expressing equilibrium and compatibility of a shell of revolution can be formulated as a set of eight simultaneous first-order differential equations. The present chapter is concerned with the formulation of suitable boundary conditions at the edges of the shell.

In order to integrate the eight Equations (41) four boundary conditions must be formulated at each end point of the interval of integration, i.e. the shell must be bounded by two edges, at $s = s_1$ and at $s = s_2$, respectively. This implies that a closed shell, e.g. a spherical cap, must be »opened» at the top, i.e. must be treated as having a small hole at the top. It will subsequently be shown how suitable boundary conditions can be formulated for this case.

For one particular Fourier term m, the most general form for the boundary conditions is the equations between boundary forces and displacements

$$\mathbf{V}\begin{bmatrix} u \\ v \\ w \\ w' \end{bmatrix} + \mathbf{D}\begin{bmatrix} N_{12} - \frac{1}{r} M_{12} \sin\phi \\ N_2 \\ Q_2 + \frac{\mathrm{m}}{r} M_{12} \\ M_2 \end{bmatrix} = \begin{bmatrix} C_1 \\ C_2 \\ C_3 \\ C_4 \end{bmatrix}$$

or

$$\mathbf{V} \cdot \mathbf{u} + \mathbf{D} \cdot \mathbf{f} = \mathbf{C} \tag{73}$$

where $\mathbf{V}$ and $\mathbf{D}$ are 4×4 coefficient matrices. In the subsequent equations the following notation will be used for the boundary forces (see [1] p. 233):

$$N_{12} - \frac{1}{r} M_{12} \sin\phi = N_{12}^{*}$$

$$Q_2 + \frac{\mathrm{m}}{r} M_{12} = Q_2^{*}$$

Now

$$\mathbf{u} = \begin{bmatrix} 1 & 0 & 0 & 0 & 0 & 0 & 0 & 0 \\ 0 & 1 & 0 & 0 & 0 & 0 & 0 & 0 \\ 0 & 0 & 1 & 0 & 0 & 0 & 0 & 0 \\ 0 & 0 & 0 & 0 & 0 & 1 & 0 & 0 \end{bmatrix} \begin{bmatrix} u \\ v \\ w \\ u' \\ v' \\ w' \\ w'' \\ Q_2 \end{bmatrix} = \mathbf{Y}_1 \cdot \mathbf{F}$$

and

$$\mathbf{f} = \begin{bmatrix} 0 & 0 & 1 & 0 & 0 & -\frac{\sin\phi}{r} & 0 \\ 0 & 1 & 0 & 0 & 0 & 0 & 0 \\ 0 & 0 & 0 & 0 & 0 & \frac{\mathrm{m}}{r} & 1 \\ 0 & 0 & 0 & 0 & 1 & 0 & 0 \end{bmatrix} \begin{bmatrix} N_1 \\ N_2 \\ N_{12} \\ M_1 \\ M_2 \\ M_{12} \\ Q_2 \end{bmatrix} = \mathbf{Y}_2\mathbf{HF}$$

(see Eq. (18)) so that (73) can be transformed to

$$\mathbf{JF} = \mathbf{C} \tag{74}$$

which is the standard and most general form of the boundary conditions. **J** is a (4 × 8)-matrix, **C** (4 × 1).

Any physically possible relationship between displacements, stress resultants and loads along the boundary, consistent with the Fourier expansion form $u = u\sin m\theta$ etc., can be expressed in the above form. The formulations for boundary conditions of special practical interest will be given below.

4.2 *Fixed edge*

The conditions are

$$\begin{bmatrix} 1 & 0 & 0 & 0 \\ 0 & 1 & 0 & 0 \\ 0 & 0 & 1 & 0 \\ 0 & 0 & 0 & 1 \end{bmatrix} \begin{bmatrix} u \\ v \\ w \\ w' \end{bmatrix} + \mathbf{0}\cdot\mathbf{f} = \mathbf{0} \tag{75}$$

i.e.

$$\mathbf{V} = \mathbf{I}, \quad \mathbf{D} = 0, \quad \mathbf{C} = 0$$

4.3 *Hinged edge*

In this case we have

$$\begin{bmatrix} 1 & 0 & 0 & 0 \\ 0 & 1 & 0 & 0 \\ 0 & 0 & 1 & 0 \\ 0 & 0 & 0 & 0 \end{bmatrix} \begin{bmatrix} u \\ v \\ w \\ w' \end{bmatrix} + \begin{bmatrix} 0 & 0 & 0 & 0 \\ 0 & 0 & 0 & 0 \\ 0 & 0 & 0 & 0 \\ 0 & 0 & 0 & 1 \end{bmatrix} \begin{bmatrix} N_{12}^{\star} \\ N_2 \\ Q_2^{\star} \\ M_2 \end{bmatrix} = \begin{bmatrix} 0 \\ 0 \\ 0 \\ 0 \end{bmatrix} \tag{76}$$

4.4 *Free edge*

$$\mathbf{0}\cdot\mathbf{u}+\begin{bmatrix}1&0&0&0\\0&1&0&0\\0&0&1&0\\0&0&0&1\end{bmatrix}\begin{bmatrix}N_{12}^{\star}\\N_2\\Q_2^{\star}\\M_2\end{bmatrix}=\begin{bmatrix}0\\0\\0\\0\end{bmatrix} \tag{77}$$

i.e.

$$\mathbf{V}=\mathbf{0},\quad \mathbf{D}=\mathbf{I},\quad \mathbf{C}=\mathbf{0}$$

4.5 *Stiffening ring at edge*

In this case we can use directly the shell-ring relations developed in Ch. 3 and expressed in Eq. (61), taking into account the fact that the ring is joined to a shell segment at one point – e.g. point A – only. Eq. (61) then yields

$$(\mathbf{QT}_{\mathrm{A}}-\mathbf{Z}_{\mathrm{A}})\,\mathbf{F}_{\mathrm{A}}=\mathbf{P} \tag{78}$$

or

$$\mathbf{JF}=\mathbf{C}$$

which is the standard form.

4.6 *Plane of symmetry perpendicular to shell axis*

When the structure and the loading have a plane of symmetry x – x as shown in Fig. 12, it will be sufficient to consider only half of the shell with the boundary conditions

$$\begin{aligned}&N_{12}-\frac{M_{12}}{r}\sin\phi=0\\&\left(Q_2-\frac{\mathrm{m}}{r}M_{12}\right)\sin\phi-N_2\cos\phi=0\\&v\sin\phi+w\cos\phi=0\\&w'=0\end{aligned} \tag{79}$$

which can be written in the form (73) and (74) as shown in the examples above.

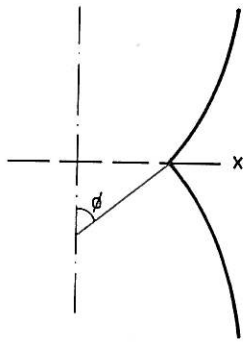

Fig. 12. The case of the structure and the loading having a plane of symmetry perpendicular to shell axis.

4.7 *Prescribed boundary loads or displacements*

A boundary load, e.g. axial prestressing P (force/unit length) may be specified as follows:

$$N_2 = P$$

If the edge is a free edge, the complete set of boundary conditions is

$$\begin{bmatrix} 1 & 0 & 0 & 0 \\ 0 & 1 & 0 & 0 \\ 0 & 0 & 1 & 0 \\ 0 & 0 & 0 & 1 \end{bmatrix} \begin{bmatrix} N_{12}^{\star} \\ N_2 \\ Q_2^{\star} \\ M_2 \end{bmatrix} = \begin{bmatrix} 0 \\ P \\ 0 \\ 0 \end{bmatrix} \tag{80}$$

Similarly a prescribed displacement, e.g. a vertical differential settlement δ of the foundation (assuming fixity in the other directions) is specified as

$$\begin{bmatrix} 1 & 0 & 0 & 0 \\ 0 & 1 & 0 & 0 \\ 0 & 0 & 1 & 0 \\ 0 & 0 & 0 & 1 \end{bmatrix} \begin{bmatrix} u \\ v \\ w \\ w^{\cdot} \end{bmatrix} = \begin{bmatrix} 0 \\ \delta \\ 0 \\ 0 \end{bmatrix} \tag{81}$$

An elastic restraint, e.g. against rotation $w^{\cdot}$ is specified as

$$M_2 \pm k w^{\cdot} = 0 \tag{82}$$

the choice of sign depending on the end at which the relation is specified.

4.8 *Closed shell*

A shell which is closed at one end, e.g. a spherical cap or a circular plate, can be considered as a shell with a small hole, the edge of which is attached to a rigid plug. Suitable boundary conditions can then be established by considering the equilibrium and the undeformability (rigid-body movement) of the plug.

The conditions can be taken as

$$\begin{aligned}
\text{m} = 0 \quad & Q_2 \cos\phi + N_2 \sin\phi = 0 \\
& v \cos\phi + w \sin\phi = 0 \\
& w^{\cdot} = 0 \\
\text{m} = 1 \quad & N_{12} + Q_2 \sin\phi - N_2 \cos\phi = 0 \\
& r Q_2 \cos\phi + r N_2 \sin\phi - M_2 = 0 \\
& u + v \cos\phi + w \sin\phi = 0 \\
& v \sin\phi - w \cos\phi + r w^{\cdot} = 0 \\
\text{m} = 2, 3 \ldots \quad & u = v = w = w^{\cdot} = 0
\end{aligned}$$

5 The integration of equations

5.1 *Survey*

In Chs. 2···4 the following sets of equations have been developed:

– the differential relations (41) relating the actions (displacements and their derivatives) of two adjacent points on the shell meridian

$$\frac{d}{ds}\mathbf{F} = \mathbf{AF} + \mathbf{B} \qquad (8 \text{ eqs.}) \tag{83}$$

– the Equations (63) relating the actions at the end points A, B of two adjacent shell elements separated by a stiffening ring

$$\mathbf{F}_B = \mathbf{G}_r \cdot \mathbf{F}_A + \mathbf{L}_r \quad (8 \text{ eqs.}) \tag{84}$$

– and finally the boundary conditions (74) that are specified at each end of the shell structure

$$\begin{aligned} \mathbf{J}_0\mathbf{F}_0 &= \mathbf{C}_0 \qquad (4 \text{ eqs.}) \text{ at end } s = s_0 \\ \mathbf{J}_n\mathbf{F}_n &= \mathbf{C}_n \qquad (4 \text{ eqs.}) \text{ at end } s = s_n \end{aligned} \tag{85}$$

The Equations (83)···(85) completely define the mathematical – or rather the computational – problem of the shell analysis. The situation is illustrated in Fig. 13 where the shell structure is schematically shown as a straight line representing the interval from $s = s_0$ to $s = s_n$.

A stiffening ring R is shown between the two shell segments. For the purpose of numerical integration, stress and displacement evaluation etc., the length $s_n - s_0$ is divided into intervals of length h, preferably a constant within each shell segment. The points 0, 1, 2... will be termed stations below. A ring or a point of discontinuity necessitates two stations, one on either side of the ring, such as points 4 and 5 in Fig. 13.

Briefly, the Equations (83)···(85) are integrated and solved by a stepwise procedure, progressing from one station (i) to the next (i+1) by forming the transfer matrix **G** and particular integral **L**

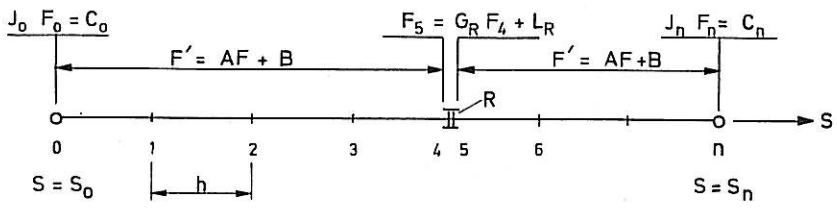

Fig. 13. The equations defining the computational problem of the shell analysis in different parts of the shell structure.

$$\mathbf{F}_{i+1} = \mathbf{G}\mathbf{F}_i + \mathbf{L} \tag{86}$$

and applying the boundary conditions at each end. However, in order to avoid problems of numerical instability, slow convergence in the series forming **G**, and ill conditioning in applying the boundary conditions, special computational techniques must be used. These techniques are described in the subsequent sections.

5.2 *The evaluation of the transfer matrix* **G** *and the particular integral* **L**

When the coefficient matrix **A** is constant over the interval h, the transfer matrix **G**, sometimes called the matrizant, equals the matrix exponential

$$\mathbf{G}(h) = e^{\mathbf{A}h} = \mathbf{I} + \mathbf{A}h/1! + \mathbf{A}^2h^2/2! + \ldots\ldots \tag{87}$$

When the load vector **B** is also constant over the interval, we have

$$\mathbf{L} = \mathbf{A}^{-1}(e^{\mathbf{A}h} - \mathbf{I})\,\mathbf{B} \tag{88}$$

which can be expanded

$$\mathbf{L} = (h\mathbf{I}/1! + h^2\mathbf{A}/2! + \ldots\ldots)\,\mathbf{B} \tag{89}$$

thereby avoiding the inversion of **A** which may be singular.

In general neither **A** nor **B** will be constant through the interval, and approximation methods must be resorted to. As explained more fully in [6] a three-point integration technique such as Runge-Kutta, which can be very satisfactory in terms of numerical accuracy will not be feasible in many practical cases, because it will require an interval size h which is much too small, and therefore too demanding with respect to computer time.

The following is a method which has been found to work very satisfactorily in practical cases.

Consider the interval i···i + 1 (Fig. 14). Let

$$\begin{aligned} \bar{\mathbf{A}} &= (\mathbf{A}_i + \mathbf{A}_{i+1})/2 \\ \bar{\mathbf{B}} &= (\mathbf{B}_i + \mathbf{B}_{i+1})/2 \end{aligned} \tag{90}$$

Compute $\mathbf{G}_1$ and $\mathbf{L}_1$, the transfer matrices from point 0 to point 1 (Fig. 14), for a small part h/k of the interval, where $k = 2^n$. Let for example $n = 3$ so that $k = 8$. $\mathbf{G}_1$ and $\mathbf{L}_1$ may then be computed with a few terms, say 6 terms, of the series (87) and (89).

We then have

$$\mathbf{F}_1 = \mathbf{G}_1\mathbf{F}_0 + \mathbf{L}_1$$

progressing to point 2

$$\mathbf{F}_2 = \mathbf{G}_1\mathbf{F}_1 + \mathbf{L}_1 = \mathbf{G}_1^2\mathbf{F}_0 + (\mathbf{G}_1 + \mathbf{I})\,\mathbf{L}_1 = \mathbf{G}_2\mathbf{F}_0 + \mathbf{L}_2$$

and from 2 to 3

$$\mathbf{F}_3 = \mathbf{G}_2\mathbf{F}_2 + \mathbf{L}_2 = \mathbf{G}_2^2\mathbf{F}_0 + (\mathbf{G}_2 + \mathbf{I})\,\mathbf{L}_2 = \mathbf{G}_3\mathbf{F}_0 + \mathbf{L}_3$$

and

$$\mathbf{F}_4 = \mathbf{G}_3\mathbf{F}_3 + \mathbf{L}_3 = \mathbf{G}_3^2\mathbf{F}_0 + (\mathbf{G}_3 + \mathbf{I})\,\mathbf{L}_3 = \mathbf{G}_4\mathbf{F}_0 + \mathbf{L}_4 \tag{91}$$

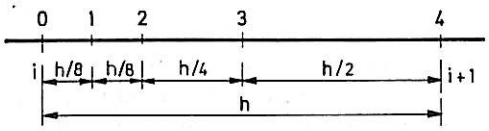

Fig. 14. Division of the interval i···i+1.

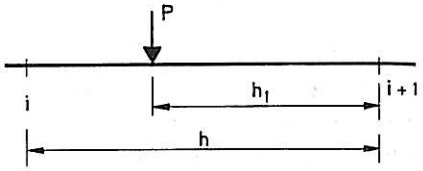

Fig. 15. A point load in the interval i···i+1.

Thus, we double the previously covered subinterval by performing one matrix multiplication, one vector multiplication and one vector addition. We have thus formed the transfer matrix for the interval h by a total of 9 matrix multiplications in this example. Forming $\mathbf{G}(h)$ directly, by series (87), might have required a much larger number of terms, depending upon the eigenvalues of $\bar{\mathbf{A}}$, as explained in [6].

The above evaluation of the particular integral holds true when $\bar{\mathbf{B}}$ can be assumed constant throughout the interval h, i.e. when we are dealing with a distributed load. When we have a discontinuous load, i.e. a point load P somewhere in the interval (see Fig. 15), the particular integral $\mathbf{L}_p$ for the point load is

$$\mathbf{L}_p = \mathbf{G}(h_1)\,\mathbf{B}_p \tag{92}$$

when $\mathbf{B}_p$ is the load vector of the point loads P_1, P_2, P_3 etc. formed as shown in Ch. 2, Eq. (35) with point loads (dimension force/unit length) instead of distributed loads (of dimension force/length^2).

5.3 *Stepwise inversion and the »bringing up» of initial conditions*

In principle, we could obtain numerical solutions to the boundary value problem defined by (83) and (85) by computing the **G** and **L** matrices for the entire shell interval $(s_n - s)$ as described above, so that we have

$$\mathbf{F}_n = \mathbf{G}\mathbf{F}_0 + \mathbf{L}$$

and then apply the boundary conditions (85) to determine the startpoint vector $\mathbf{F}_0$ by solving the system

$$\left[\begin{array}{c}\mathbf{J} \\ \hline \mathbf{J}_n\mathbf{G}\end{array}\right]\mathbf{F}_0 = \left[\begin{array}{c}\mathbf{C}_0 \\ \hline \mathbf{C}_n - \mathbf{J}_n\mathbf{L}\end{array}\right] \tag{93}$$

Having found $\mathbf{F}_0$ we have transformed the problem to an initial-value problem and can then proceed step by step to compute $\mathbf{F}_1, \mathbf{F}_2 \ldots$ at the subsequent stations.

There are two reasons, however, why this method will not work in most practical cases. Firstly, the system (93) may be highly ill-conditioned, and the more so, the longer the interval $(s_n - s_0)$. Secondly, even if we manage to determine $\mathbf{F}_0$ with acceptable accuracy, roundoff- or truncation errors may be propagated to such a degree that the subsequent evaluation of the vectors $\mathbf{F}_i$ becomes increasingly erroneous. These phenomena are explained in greater detail in [6].

We shall outline a technique of stepwise »bringing up» of initial conditions below.

By a physical analogy this is equivalent to regarding each station i as the initial one, and the connection to the shell behind as a new set of boundary conditions.

From the vector $\mathbf{F}$ we form two subvectors $\bar{\mathbf{F}}$ and $\underline{\mathbf{F}}$, each (4×1),

$$\bar{\mathbf{F}} = \begin{bmatrix} u & + u^{\cdot} \\ v & + v^{\cdot} \\ w & + Q_2 \\ w^{\cdot} & + w^{\cdot\cdot} \end{bmatrix} = \begin{bmatrix} 1 & 0 & 0 & 1 & 0 & 0 & 0 & 0 \\ 0 & 1 & 0 & 0 & 1 & 0 & 0 & 0 \\ 0 & 0 & 1 & 0 & 0 & 0 & 0 & 1 \\ 0 & 0 & 0 & 0 & 0 & 1 & 1 & 0 \end{bmatrix} \begin{bmatrix} u \\ v \\ w \\ u^{\cdot} \\ v^{\cdot} \\ w^{\cdot} \\ w^{\cdot\cdot} \\ Q_2 \end{bmatrix} = \bar{\mathbf{Q}}\mathbf{F} \tag{94}$$

$$\underline{\mathbf{F}} = \begin{bmatrix} u & - u^{\cdot} \\ v & - v^{\cdot} \\ w & - Q_2 \\ w^{\cdot} & - w^{\cdot\cdot} \end{bmatrix} = \underline{\mathbf{Q}}\mathbf{F}$$

Then

$$\mathbf{F} = \begin{bmatrix} \bar{\mathbf{Q}} \\ \underline{\mathbf{Q}} \end{bmatrix}^{-1} \begin{bmatrix} \bar{\mathbf{F}} \\ \underline{\mathbf{F}} \end{bmatrix} = [\bar{\mathbf{R}} \,|\, \underline{\mathbf{R}}] \begin{bmatrix} \bar{\mathbf{F}} \\ \underline{\mathbf{F}} \end{bmatrix}$$

$$\mathbf{F} = \bar{\mathbf{R}}\bar{\mathbf{F}} + \underline{\mathbf{R}}\underline{\mathbf{F}} \tag{95}$$

The boundary conditions in the first Equation (85) give

$$\mathbf{J}_0(\bar{\mathbf{R}}\bar{\mathbf{F}}_0 + \underline{\mathbf{R}}\underline{\mathbf{F}}_0) = \mathbf{C}_0$$

whence

$$\underline{\mathbf{F}}_0 = (\mathbf{J}_0\underline{\mathbf{R}})^{-1}(\mathbf{C}_0 - \mathbf{J}_0\bar{\mathbf{R}}\bar{\mathbf{F}}_0)$$

Eq. (95) gives

$$\mathbf{F}_0 = \bar{\mathbf{R}}\bar{\mathbf{F}}_0 + \underline{\mathbf{R}}(\mathbf{J}_0\underline{\mathbf{R}})^{-1}(\mathbf{C}_0 - \mathbf{J}_0\bar{\mathbf{R}}\bar{\mathbf{F}}_0)$$

which can be arranged thus

$$\mathbf{F}_0 = \mathbf{K}_0\bar{\mathbf{F}}_0 + \mathbf{V}_0 \tag{96}$$

where $\mathbf{K}$ is (8×4) and $\mathbf{V}$ (8×1).

We have now succeeded in expressing the full vector $\mathbf{F}_0$ at the starting point by 4 linear combinations $\bar{\mathbf{F}}_0$ of $\mathbf{F}_0$. We shall proceed to show how we can obtain an identical representation at any station i.

We integrate (83) over the interval h as explained in Section 5.2 and obtain

$$\mathbf{F}_1 = \mathbf{G}\mathbf{F}_0 + \mathbf{L} \tag{97}$$

Using (96) we get

$$\mathbf{F}_1 = \mathbf{G}(\mathbf{K}_0\bar{\mathbf{F}}_0 + \mathbf{V}_0) + \mathbf{L} = \mathbf{T}\bar{\mathbf{F}}_0 + \mathbf{U} \tag{98}$$

Using (94)

$$\bar{\mathbf{F}}_1 = \bar{\mathbf{Q}}\mathbf{T}\bar{\mathbf{F}}_0 + \bar{\mathbf{Q}}\mathbf{U} = \bar{\mathbf{T}}\bar{\mathbf{F}}_0 + \bar{\mathbf{U}}$$

yielding

$$\bar{\mathbf{F}}_0 = \bar{\mathbf{T}}^{-1}(\bar{\mathbf{F}}_1 - \bar{\mathbf{U}}) \tag{99}$$

By (98) we can now express $\mathbf{F}_1$ in terms of $\bar{\mathbf{F}}_1$

$$\mathbf{F}_1 = \mathbf{T}\bar{\mathbf{T}}^{-1}(\bar{\mathbf{F}}_1 - \bar{\mathbf{U}}) + \mathbf{U}$$

or

$$\mathbf{F}_1 = \mathbf{K}_1\bar{\mathbf{F}}_1 + \mathbf{V}_1 \tag{100}$$

The form (100) is identical to the form (96) at the starting point, and we can therefore say that we have »brought up» the initial conditions.

We proceed, as above, step by step until we reach the other edge of the shell where we have

$$\mathbf{F}_n = \mathbf{K}_n\bar{\mathbf{F}}_n + \mathbf{V}_n \tag{101}$$

and by using the boundary conditions of the second Equation (85) we get

$$\bar{\mathbf{F}}_n = (\mathbf{J}_n\mathbf{K}_n)^{-1}(\mathbf{C}_n - \mathbf{J}_n\mathbf{V}_n) \tag{102}$$

whence $\mathbf{F}_n$ is found by (101).

Having determined the function vector $\mathbf{F}$ at the edge n we can now compute the succession of vectors $\mathbf{F}_{n-1}$, $\mathbf{F}_{n-2}\cdots\mathbf{F}_0$ by making use of the recurrence relation

$$\mathbf{F}_{i-1} = \mathbf{K}_{i-1}\bar{\mathbf{T}}^{-1}(\bar{\mathbf{F}}_i - \bar{\mathbf{U}}) + \mathbf{V}_{i-1}$$

or

$$\mathbf{F}_{i-1} = \mathbf{H}_{i-1}\bar{\mathbf{F}}_i + \mathbf{W}_{i-1} \tag{103}$$

The (8×4) matrices $\mathbf{H}$ and the (8×1) vectors $\mathbf{W}$ can readily be formed during the forward integration and stored.

6 The cooling towers at Ferrybridge

6.1 *Introduction*

As mentioned in the introduction, the author's work with shells of revolution originated with an analysis of the failure, in a wind storm, of the three hyperbolic cooling towers at Ferrybridge, England, on November 1, 1965. In an attempt to determine the stresses in the shells at the time of failure according to bending theory, the method of analysis given in the previous chapters was developed and a computer programme for the Pegasus computer then in operation at Southampton University was written.

6.2 *Model for analysis*

The geometry and main dimensions of the towers are shown in Fig. 16. The towers are supported on a set of inclined columns as shown, providing an elastic restraint along the lower edge, where the boundary conditions will express the force-displacement relations of the supporting columns, as explained in principle in Section 4.7 above.

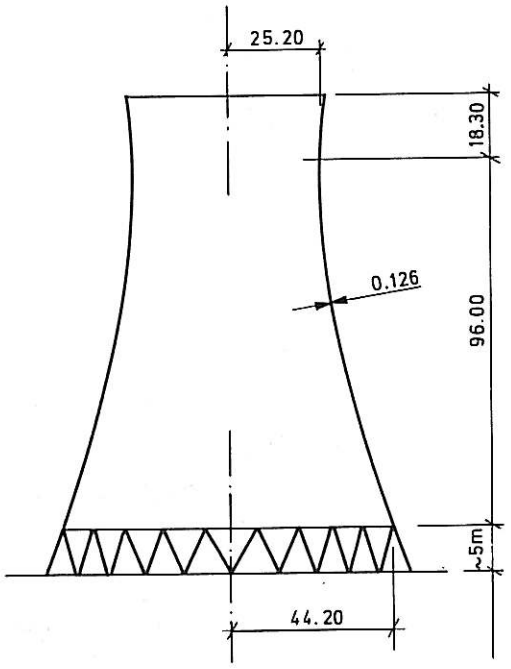

Fig. 16. The geometry and main dimensions of the towers.

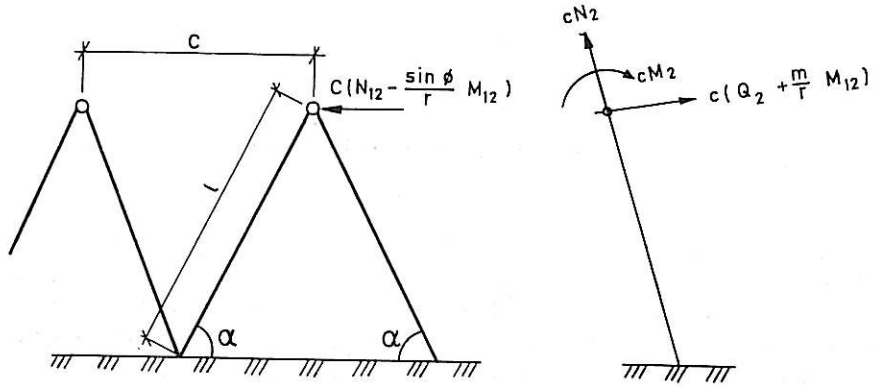

Fig. 17. The forces acting on the columns.

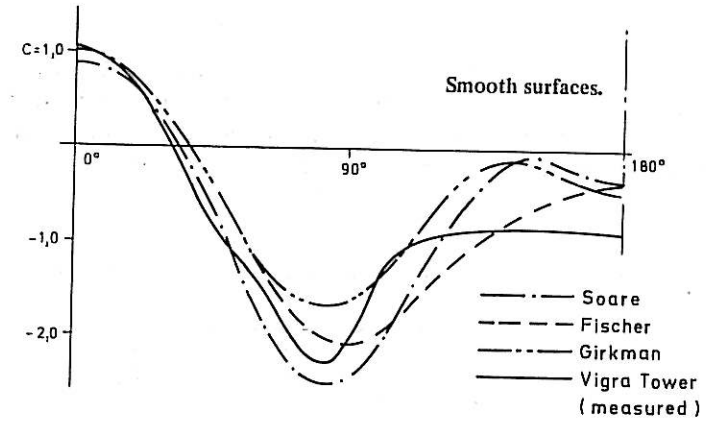

$$p = c \cdot p_o$$

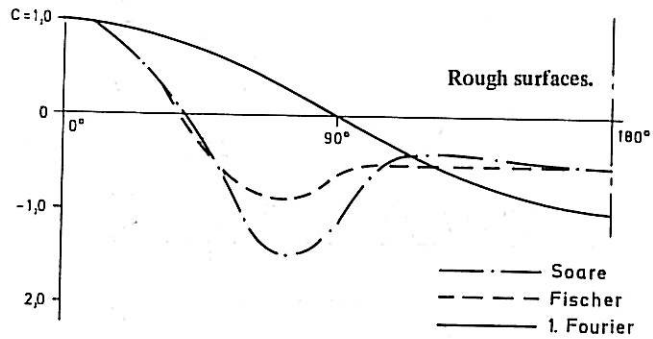

Fig. 18. Wind pressure on cylinder.

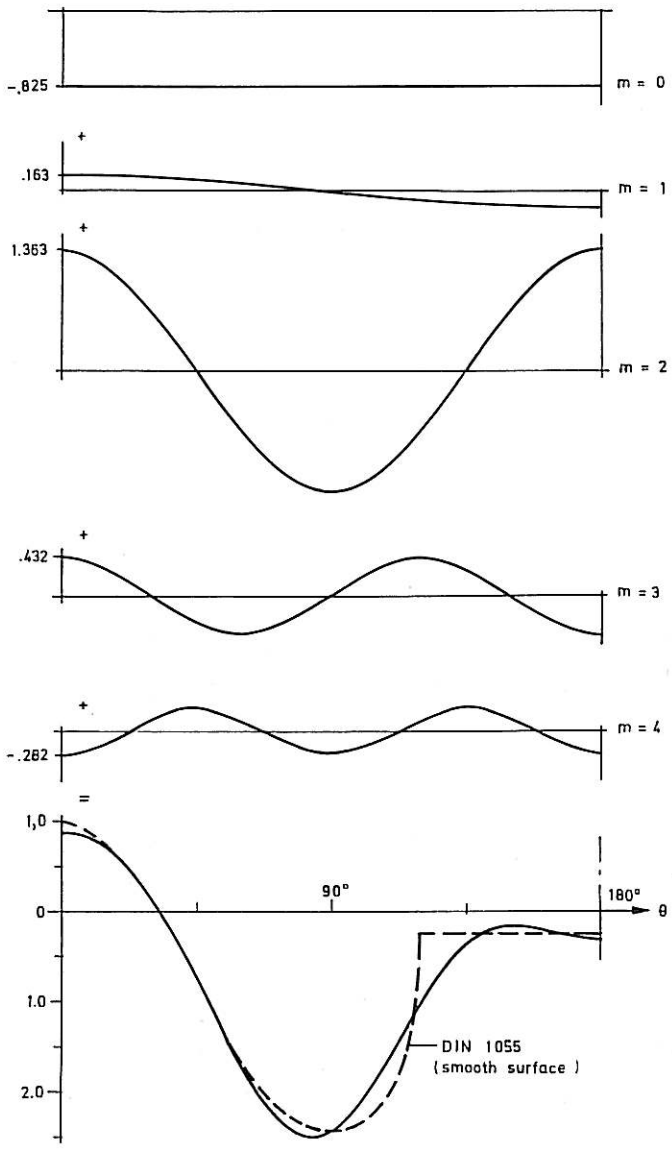

Fig. 19. Fourier synthesis of wind pressure.

A consideration of the displacements at the shell/column junction and the force/stiffness relationships of the columns give the boundary equations

$$\begin{bmatrix} 1 & 0 & 0 & 0 \\ 0 & 1 & 0 & 0 \\ 0 & 0 & 1 & 0 \\ 0 & 0 & 0 & 1 \end{bmatrix} \mathbf{u} + \begin{bmatrix} \frac{lc}{AE\cos^2\alpha} & 0 & 0 & 0 \\ 0 & \frac{lc}{AE\sin^2\alpha} & 0 & 0 \\ 0 & 0 & -\frac{cl^3}{3EI} & -\frac{cl^2}{2EI} \\ 0 & 0 & \frac{cl^2}{2EI} & \frac{cl}{EI} \end{bmatrix} \mathbf{f} = 0 \tag{104}$$

where AE and EI are the axial and bending stiffness of a pair of columns, respectively, other symbols are given in Figs. 16 and 17, where the forces acting on the columns are also shown.

6.3 *Wind load*

The estimation of a reasonably realistic wind pressure at a given point in time on the structure shown in Fig. 16 is a very complex matter, as a number of factors whose effect is incompletely understood have to be considered. For a treatment of the subject, the reader is referred to [7], where a number of wind tunnel tests are reported.

Some distributions for the pressure variations around cylindrical bodies recommended by various authors appear in Fig. 18. The Fourier expansions for some of these distributions are given in Table 1.

Table 1. Fourier expansions of wind pressure around cylinder.

rough surfaces	m =	0	1	2	3	4
DIN 1055		−0,237	0,488	0,425	0,329	0,118
Soare		−0,258	0,488	0,476	0,378	0,100
smooth surfaces	**m =**	**0**	**1**	**2**	**3**	**4**
DIN 1055		−0,838	0,234	1,318	0,322	−0,060
Soare		−0,804	0,140	1,380	0,490	−0,318
Girkman		−0,526	0,253	0,950	0,462	−0,189

A typical Fourier synthesis is shown in Fig. 19.

6.4 *Results*

Some selected results are shown in Figs. 20···23. The diagrams in Fig. 20 showing the meridional force N_2 and bending moment M_2 for the individual Fourier load terms indicate the sensitivity of the shell to local loads. The load $p = 1{,}0 \cos 5\theta$, for example,

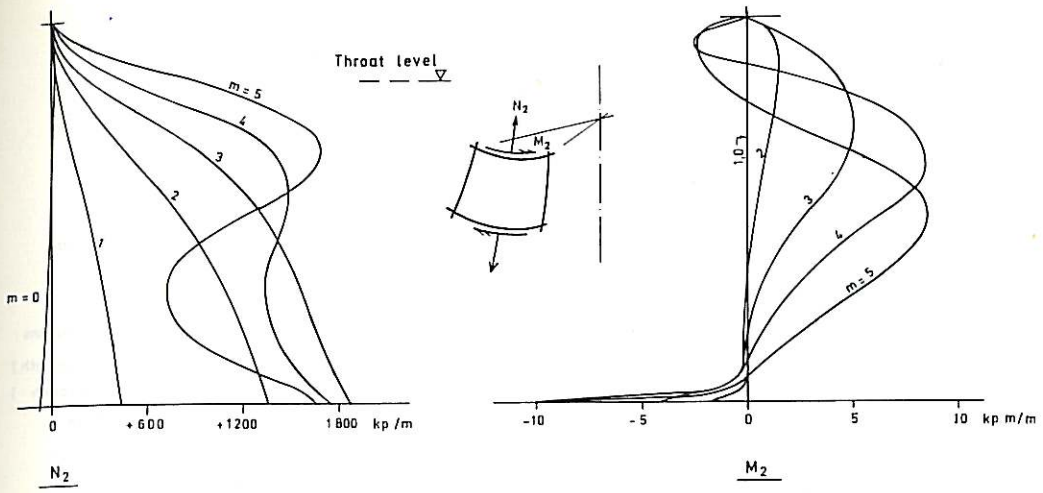

Fig. 20. Stress resultants N_2 and M_2 for $p = 1 \cdot \cos m\theta$.

can only have local effects, as it is self-equilibrating over a sector spanning from $\theta = 0$ to $\theta = 2\pi/5$. These local effects, however, are very considerable and in fact quite dominant, as shown by Fig. 20. Similar pictures have been obtained for the other stress resultants, and for N_1 this tendency to high local stresses was even more pronounced.

The resulting circumferential (N_1, M_1) and meridional (N_2, M_2) stress resultants along two different meridians and for three different pressure distributions are given in Figs. 21 and 22. The differences, which are considerable, are due not so much to different estimations of the total wind resultant which is represented by the $\cos\theta$-term whose effect is rather modest, but rather to the different appreciations of the higher Fourier terms and the local effects stemming from these.

The concluding diagram, Fig. 23, shows the resulting maximum meridional and circumferential force as a combination of wind and dead load. It can be seen that if only the wind load resultant force as represented by the $p\cos\theta$-term is considered, the shell remains under vertical compression, and a minimum reinforcement is all that is needed in the vertical direction. If, however, more realistic pressure distributions are used where the high local suctions on the sides are considered, the picture of vertical stress changes radically from compression to tension of more than 30 t/m, requiring considerable amounts of vertical reinforcement.

Since the author's results on the Ferrybridge Tower analysis first appeared in a report of March, 1966 [5], a considerable amount of theoretical and experimental results have been compiled, and it may be of interest to quote the conclusion of the Committee of enquiry in its report of August, 1966 [7]:

»The Committee find that the tower failures at Ferrybridge were primarily caused by a serious underestimate of the wind loading in the design, which led to tensile failure of the vertical reinforcement in the lower part of the shells..... Wind loading deficiencies in both the specification and design were aggravated by a mistaken interpretation of the pressure distribution data.«

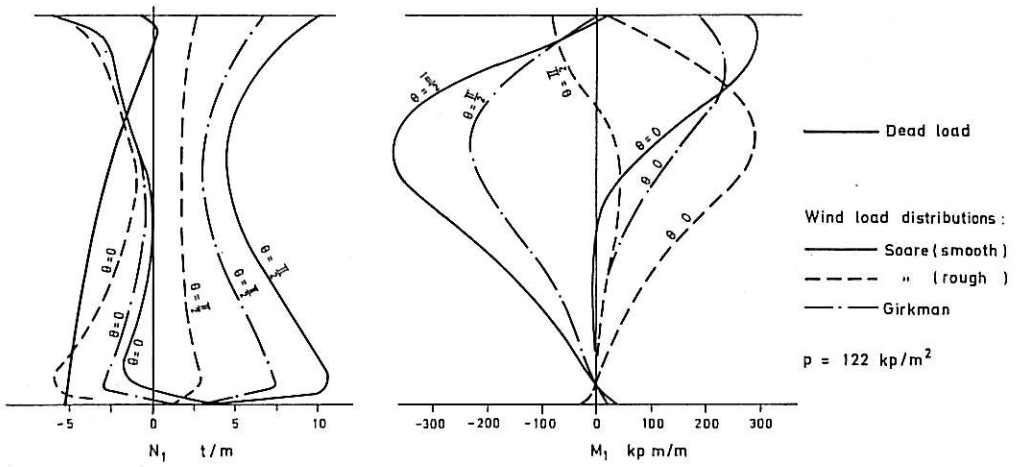

Fig. 21. Stress resultants N_1 and M_1.

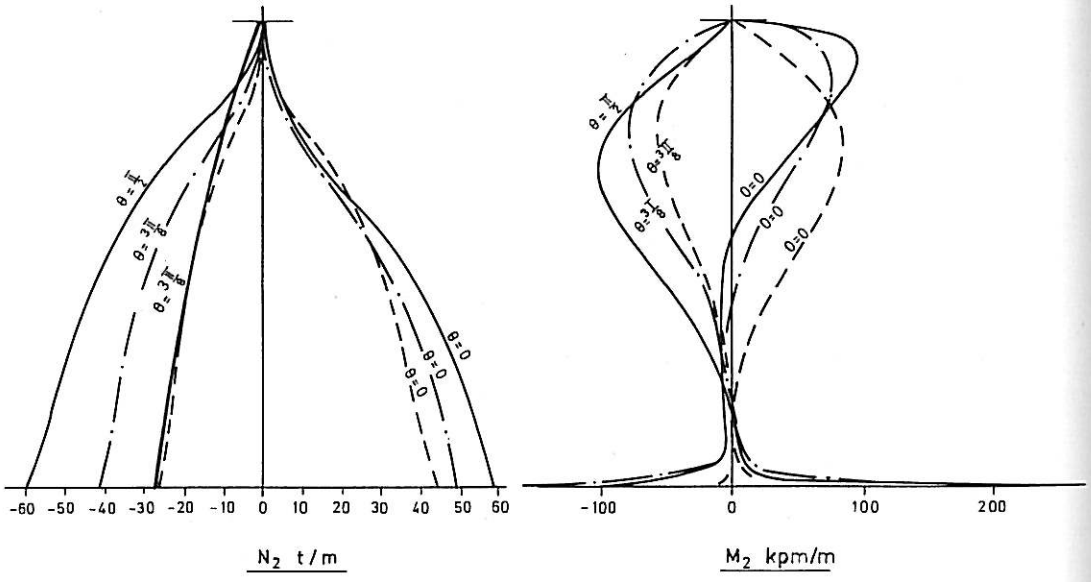

Fig. 22. Stress resultants N_2 and M_2.

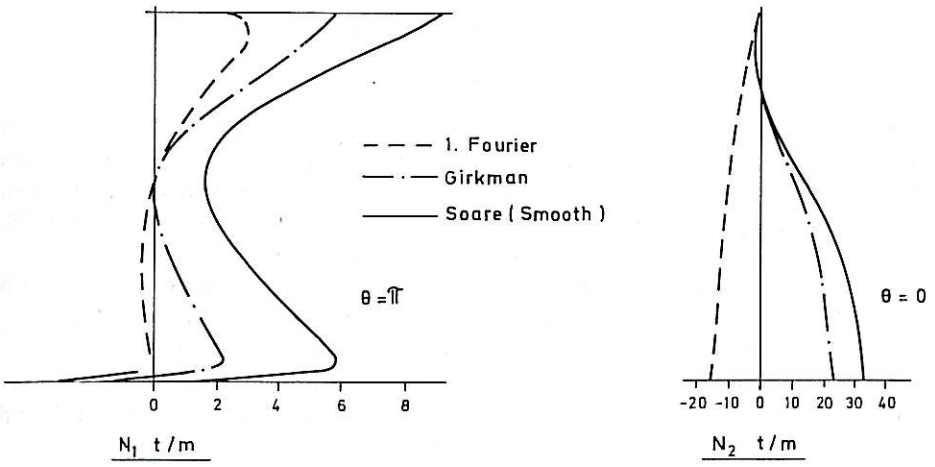

Fig. 23. Total resulting N_1 and N_2, wind and dead load combined.

7 Two further examples

7.1 *Skewly filled silo*

An unsymmetrical load of practical significance is the wall pressure in a silo which is filled skewly, as may well happen. The situation is illustrated in Fig. 24 which shows a reinforced concrete silo skewly filled with soya beans. The estimated radial load on the silo walls, as approximated by a Fourier series of 8 terms, is indicated in Fig. 25. There is a simultaneous vertical surface load, equal to 1/3 of the radial load.

The significance of the skewness of the loading as compared to an axisymmetric load B (horizontal filling surface) is illustrated in Fig, 26a···c. While the circumferential force N_1 is practically unaffected, substantial ring bending moments M_1 arise in the skew case, calling for large amounts of reinforcement. Unless the skew loading case is considered in the analysis, it is not likely that sufficient bending reinforcement will be provided, and cracking may occur in the upper part of the silo during use.

7.2 *Conical shell with point loads*

Fig. 27 shows a silo for coke, 38 m in height, with a roof in the form of a truncated cone. The 15 cm thick conical shell roof supports a bridge for the means of filling. Wind pressure on the bridge gives rise to an antimetric set of vertical point loads, as shown in Fig. 27b. The point loads are approximated by a Fourier series as shown in Fig. 27c.

Some results are shown on Figs. 27d···f. The point loads create high local bending moments as well as high membrane forces in the θ direction.

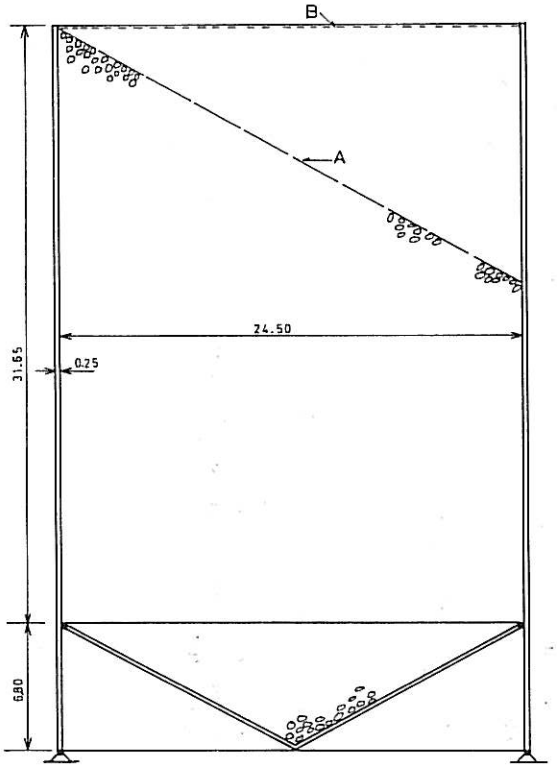

Fig. 24. Silo, vertical section.

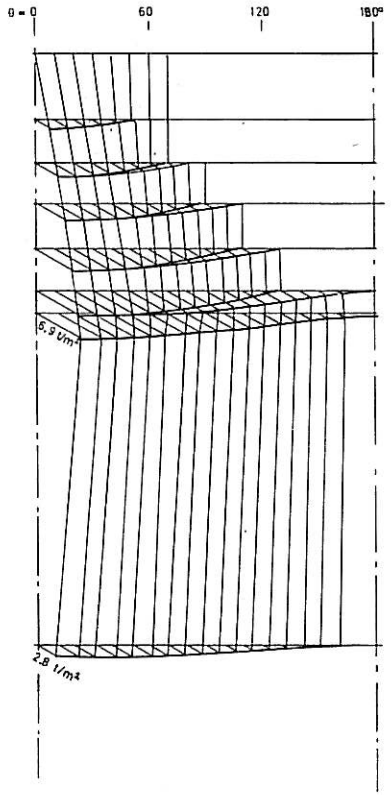

Fig. 25. Radial load on silo wall.

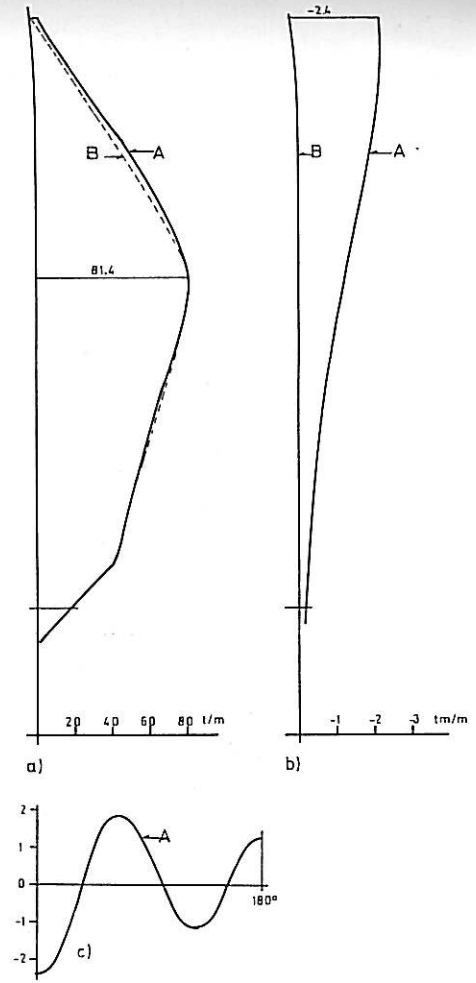

Fig. 26. a) N_1 along $\theta = 0$, b) M_1 along $\theta = 0$, c) M_1 along upper edge.

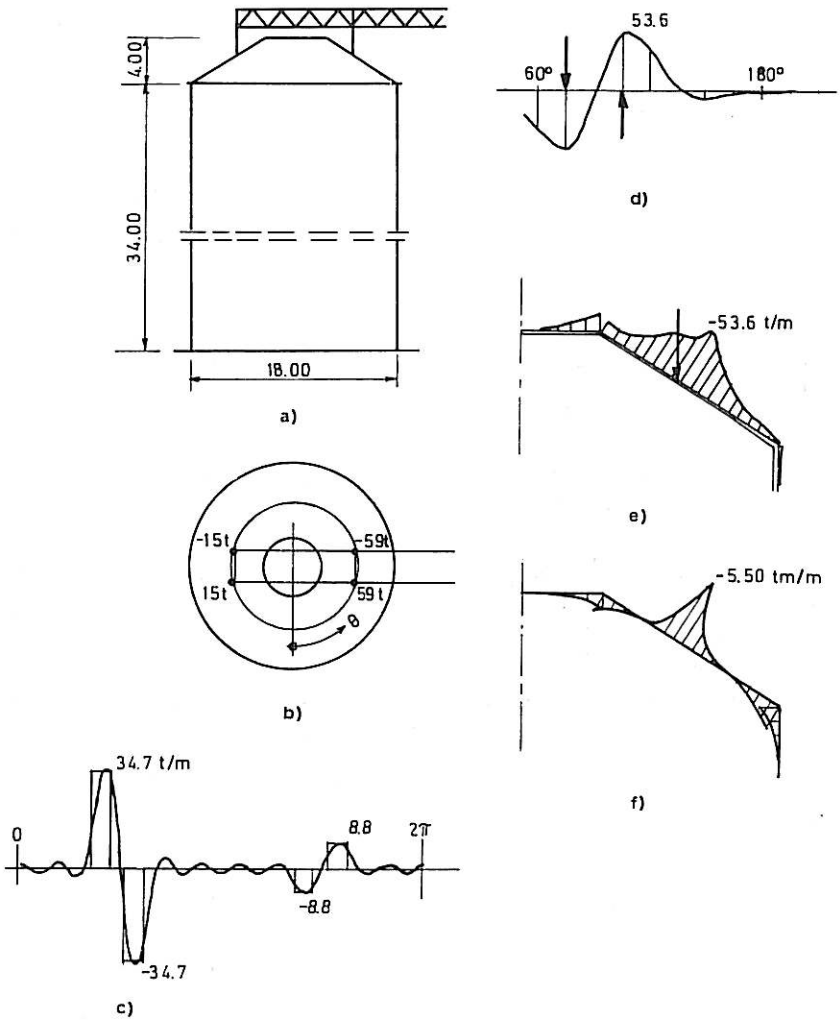

Fig. 27. Point loads on conical shell.
a) Silo, b) Point loads, c) Load approximation, d) N_2 along circle,
e) N_2 along meridian, f) M_2 along meridian.

8 Analysis of a ball valve housing

by Dipl.Eng. Odd Biberg*

8.1 *Introduction*

A ball valve for a hydro-electric installation of the type designed and produced by Kværner Brug A/S – Oslo appears in Fig. 28. Such valves have been delivered to the hydro-electric plants at Tonstad, Trollheimen, Norway, and to Kafue Gorge, Zambia.

The valve body, which is mounted for rotation about the boss axis, transfers a total water pressure force of $P_{max} = 2{,}5 \cdot 10^6$ kp – 2500 tons – to the spherical shell through the bosses when the valve is closed. The shell structure is rotationally symmetric except for the bosses, where concentrated loads are induced.

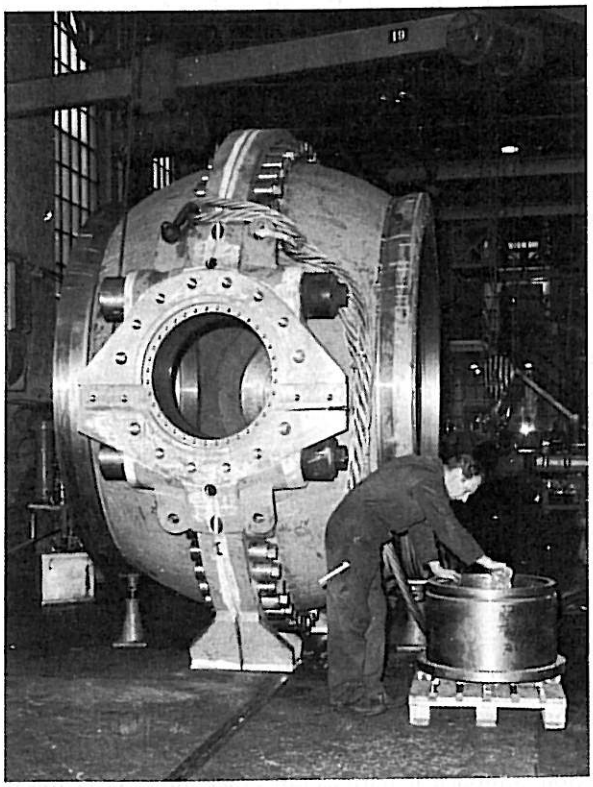

Fig. 28. Ball valve housing.

* Turbine Department, Kværner Brug A/S – Oslo

Important dimensioning parameters, such as the ovality of the flange packings and the stresses in certain points of the shell are known for this type of non-symmetric load from an approximate analysis and from measurements on existing structures. In order to obtain a complete picture of stresses and deformations, an analysis with the computer programme RSHELL was carried out. This programme was selected because it has simple model generation and input (about one day's work for the example described) and required little computing time (about 90 seconds on a Univac 1108).

A number of valves with varying dimensions and in different pressure-classes in the delivery-programme could be analyzed.

Since the RSHELL-model also includes the penstock, the analysis has contributed to an understanding of the important interaction between valve housing and penstock. Furthermore, the RSHELL-analysis has made it possible to optimize the shell radius with regard to the stresses in shell penstock in the transition zone.

8.2 *Description of the model*

The mathematical model is shown in Fig. 29, and consists of

cylindrical pipe (penstock), station	1 – 2
transition zone (flange packings), station	2 – 7
spherical shell (valve housing), station	7 – 9
transition zone (flange packings), station	9 – 13
end pipe (expansion box), station	13 – 14.

The segment between stations 3 and 4 is a »simulator element» for the pipe flange, the analogue behaviour of which has been verified by a finite-element analysis of the true flange.

The loads are shown in Fig. 30. These are

- internal water pressure
- concentrated forces at the bosses, modelled as distributed surface loads in the boss areas
- loads compensating for the difference between the actual physical contour and the theoretical model contour.

The Fourier analysis and resulting synthesis of the concentrated boss-loads is shown in Fig. 30b.

8.3 *Results*

Fig. 31 shows the circumferential variation of the meridional membrane force N_2 in a section through the bosses (point 8) and away from the bosses (point 7), the bosses lying at $\theta = 0°$ and $\theta = 180°$. As might be expected, there is a considerable variation in N_2 in the boss-section, although it flattens out as we move away towards the end zones of the shell. In other words, the higher Fourier terms, which appear to contribute substantially to the stress field in point 8, are quickly dampened out. This often occurs in a shell with positive Gaussian curvature.

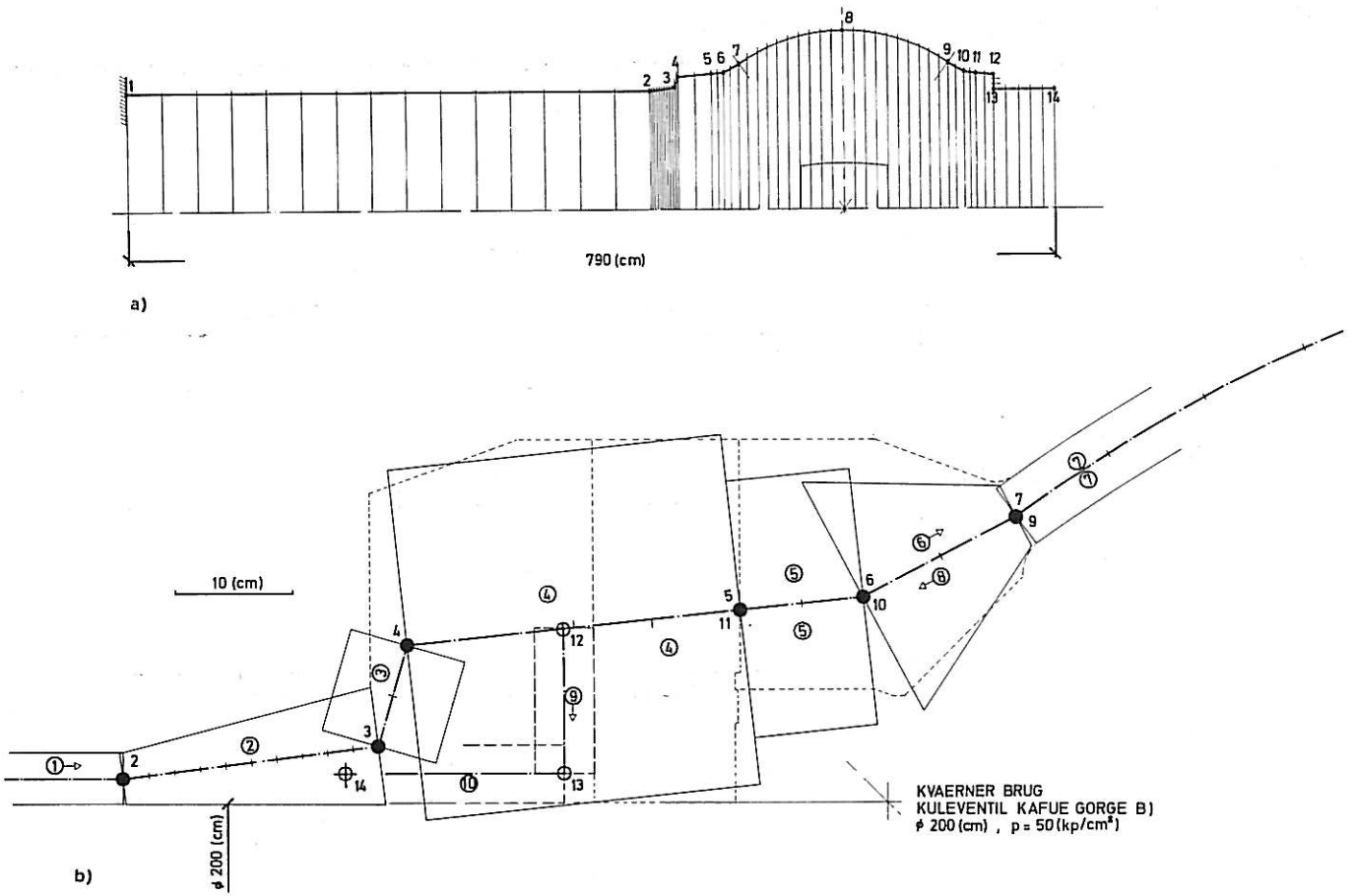

Fig. 29. a) RSHELL model; penstock, flanges and valve housing, b) Transition zone, detail.

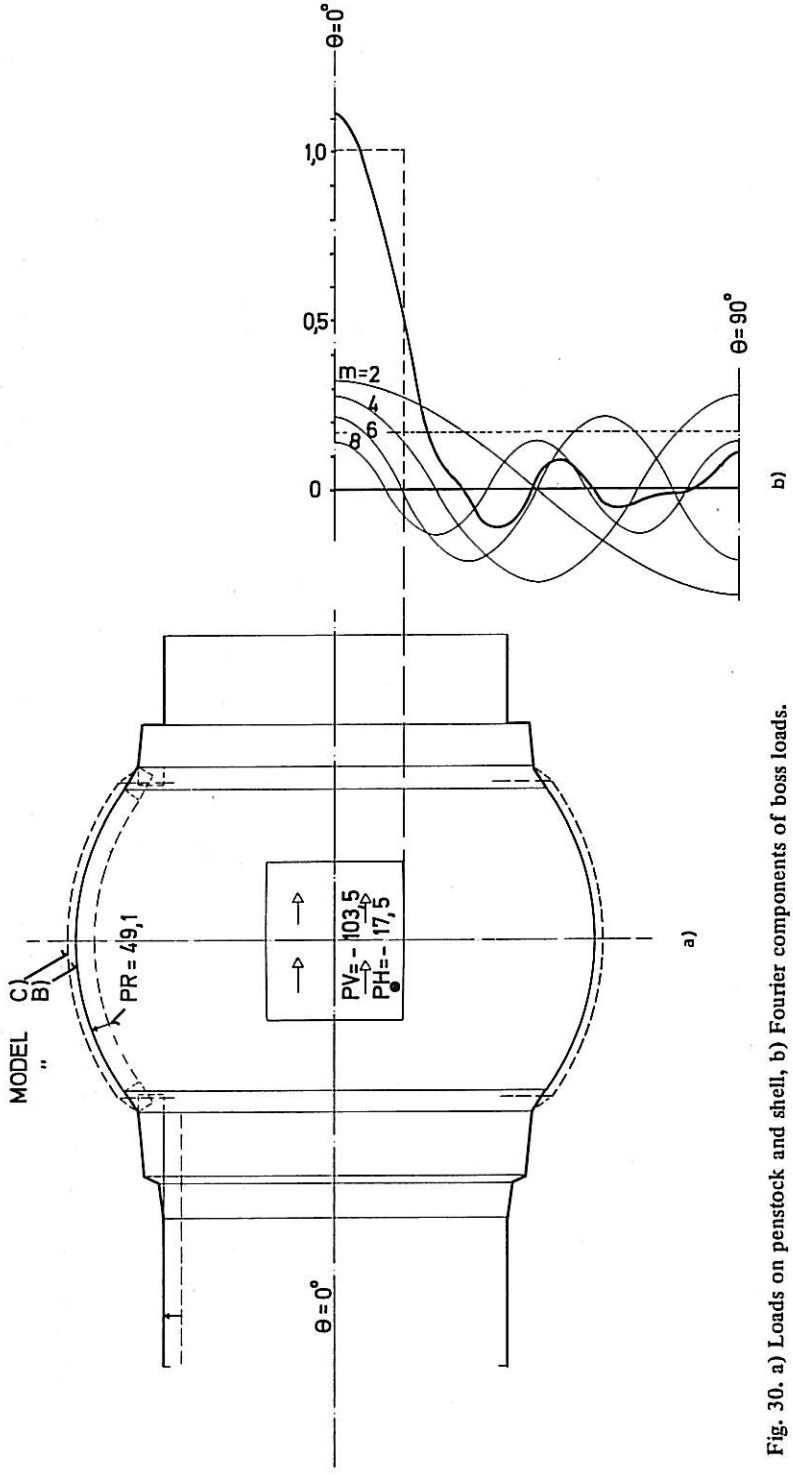

Fig. 30. a) Loads on penstock and shell, b) Fourier components of boss loads.

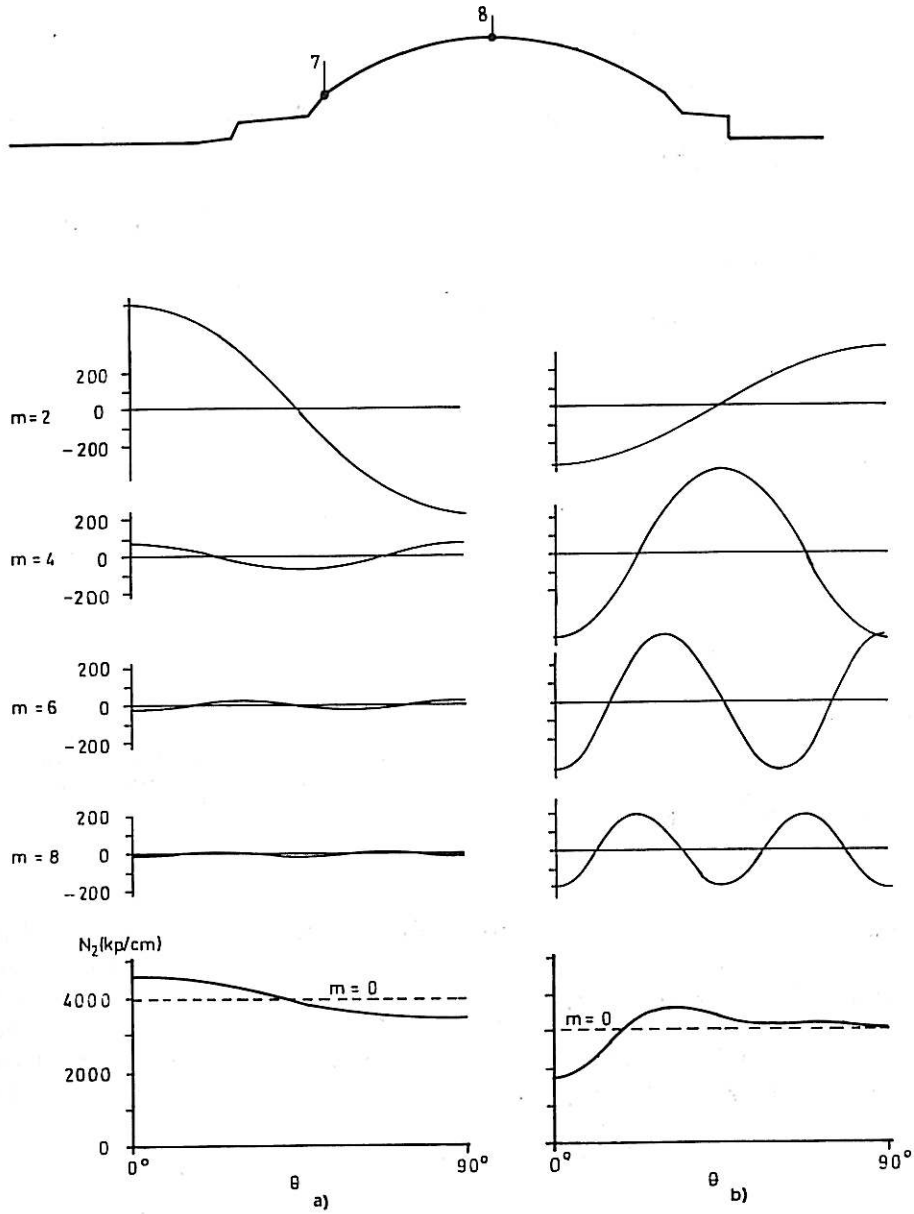

Fig. 31. Membrane force N_2. a) at point 7, b) at point 8.

Fig. 32a shows resulting surface stresses σ along the generating curves $\theta = 0$ and $\theta = 90^\circ$ in the meridional direction. Fig. 32b shows a comparison between computed stresses at the shell-flange transition and strain-gauge measurements on the actual structure after installation and under the full water pressure.

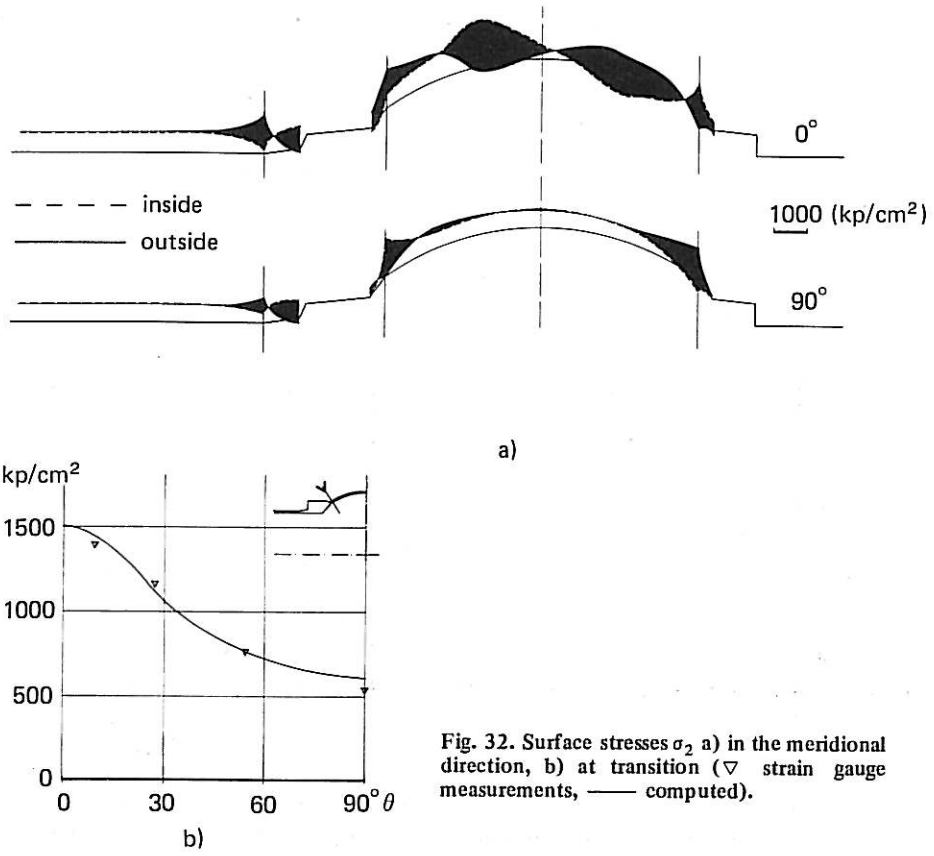

Fig. 32. Surface stresses σ_2 a) in the meridional direction, b) at transition (▽ strain gauge measurements, —— computed).

Displacement measurements on the flanges were also carried out in the power plant as the water was admitted into the penstock and valve. The water reduced the temperature of the steel by an estimated 14°C. Compensation for the accompanying dimensional changes was made in the results plotted in Fig. 33. There is substantial agreement between the computed and measured values, both with regard to radial displacement and with regard to flange warping, as indicated by the slopes of the lines 10···12 in Fig. 33.

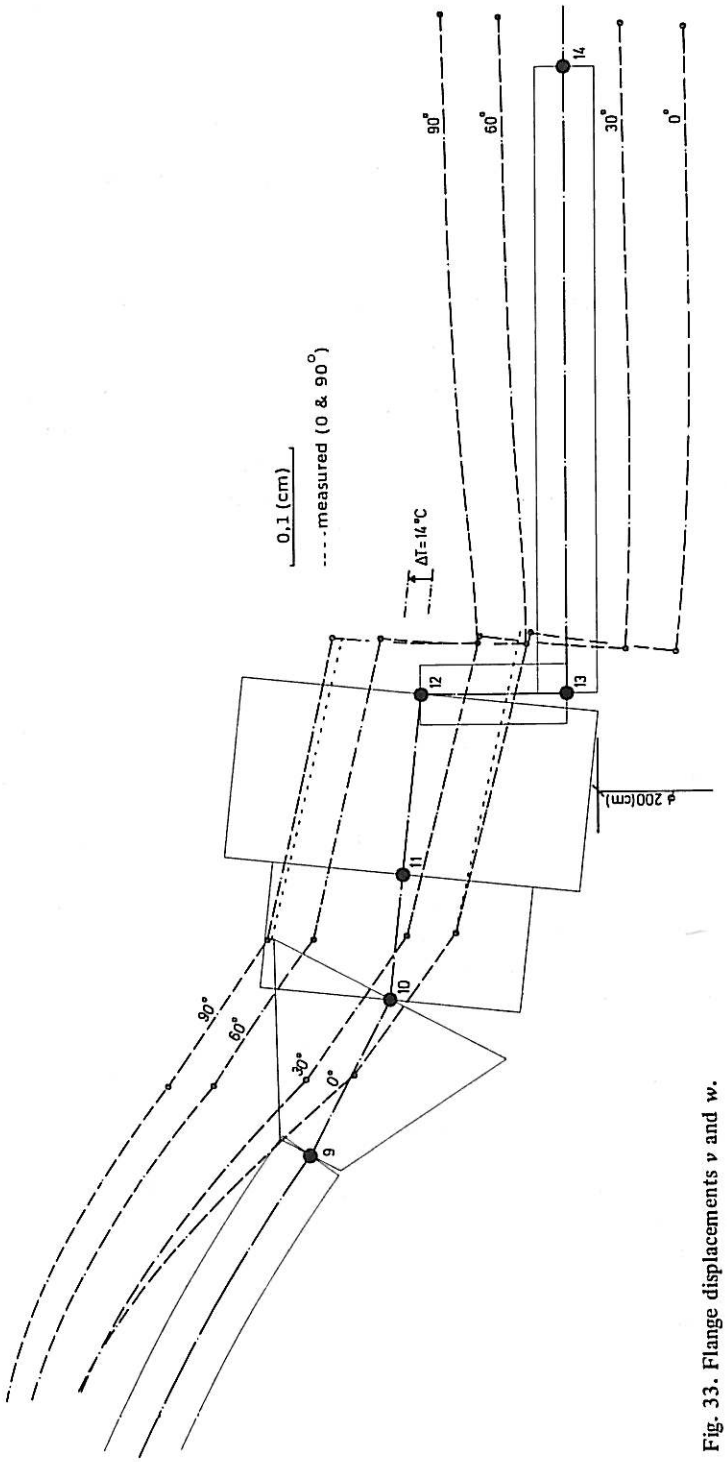

Fig. 33. Flange displacements v and w.

9 Analysis of spheres by means of the RSHELL computer programme – two examples

(by Det norske Veritas – Research Division)

9.1 *Stress analysis of sphere top with dome*

A large aluminium sphere with a dome welded to the top is subjected to internal pressure. The RSHELL computer programme was used to calculate the stresses in the dome and sphere.

The model used is shown in Fig. 34. Segments No. 1, 2, 3 form the dome cap which is a spun torispherical head. Segments No. 4, 5 are the cylindrical parts of the dome, and segments No. 6, 7 form the upper part of the sphere. The cylindrical part of the dome, which penetrates into sphere, is modeled as an inside ring.

The relations between the different geometrical parameters are

$$R_3/R_2 = 80\ ; \qquad R_3/R_1 = 1{,}8\ ; \qquad R_3/R_D = 8{,}5$$

$$t_3/t_2 = 2{,}4\ ; \qquad t_3/t_1 = 1{,}18\ ; \qquad t_1/t_2 = 2{,}07$$

Because the stresses in the dome region are of primary interest it has not been necessary to model the whole sphere.

In Figs. 35 and 36 the stresses calculated by the programme are plotted. Definition of stresses σ_ϕ and σ_θ is given in Fig. 35.

The calculations show significant increase in stresses at the corners. The stress peaks due to the bending moments at the corners are, however, very local. When moving away from the corners, the stresses soon approach the membrane theory solution.

Due to the small hole at the cap top which must be introduced, the stress picture in this region is not correct. But as we know the stresses approach the membrane theory solution, the correct stresses may be scattered with satisfactory accuracy.

Computing time was approximately 15 seconds.

9.2 *Calculation of stresses in the region of thickness transition*

It is of interest to find the effect on the membrane forces and moments of a transition between two plates with great difference in thickness in a sphere under internal overpressure compared with a transition with a plate in which there is gradually increasing plate thickness, Figs. 37a and b.

The models used are shown in Fig. 37.

Boundary condition:

upper edge (node 6) HINGED
lower edge (node 1) HINGED.

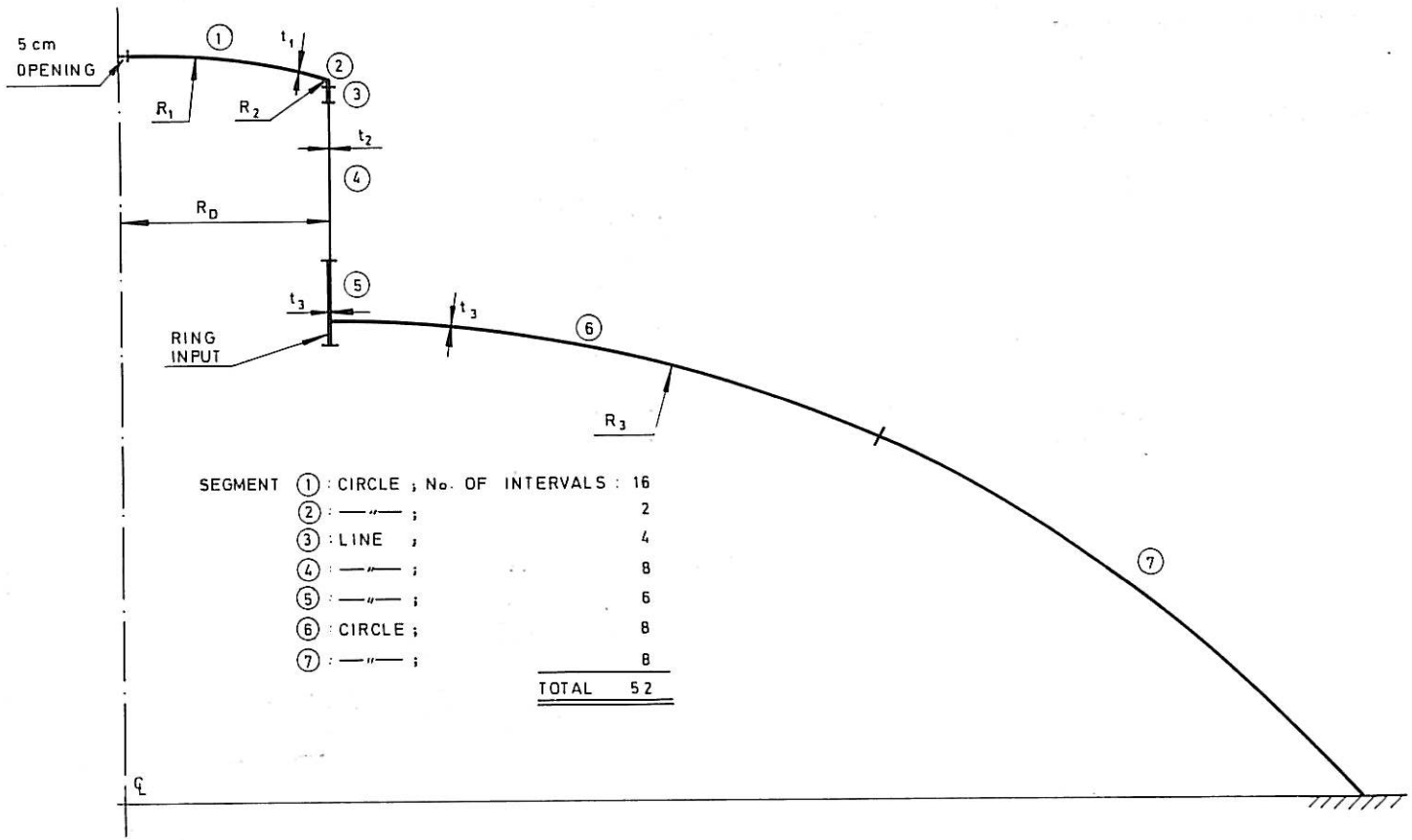

Fig. 34. Sphere top with dome. Model used in RSHELL computer program. (Load: internal pressure. Boundary conditions: Upper boundary free. Lower boundary fixed.)

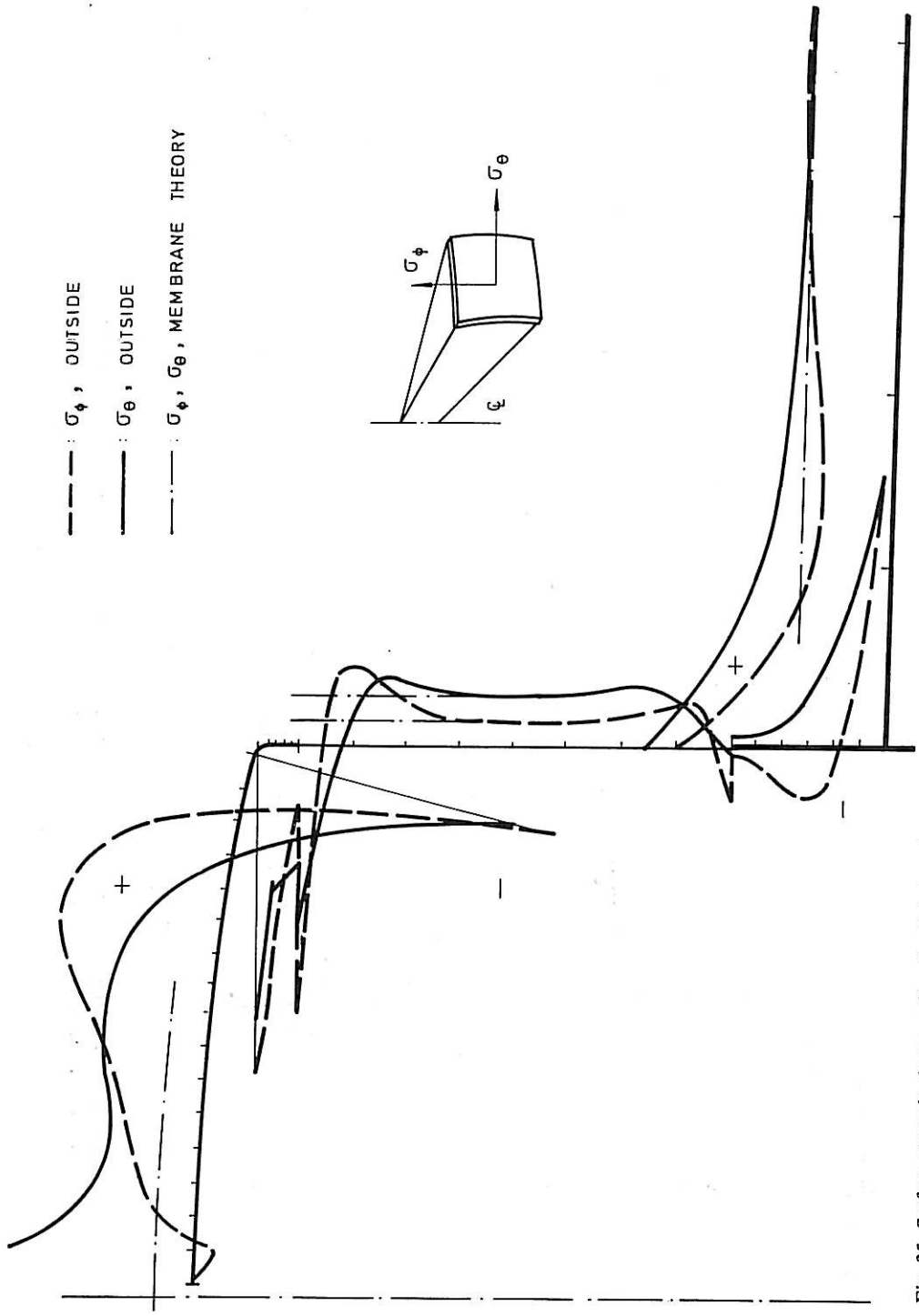

Fig. 35. Surface stress in dome region. Load: internal pressure.

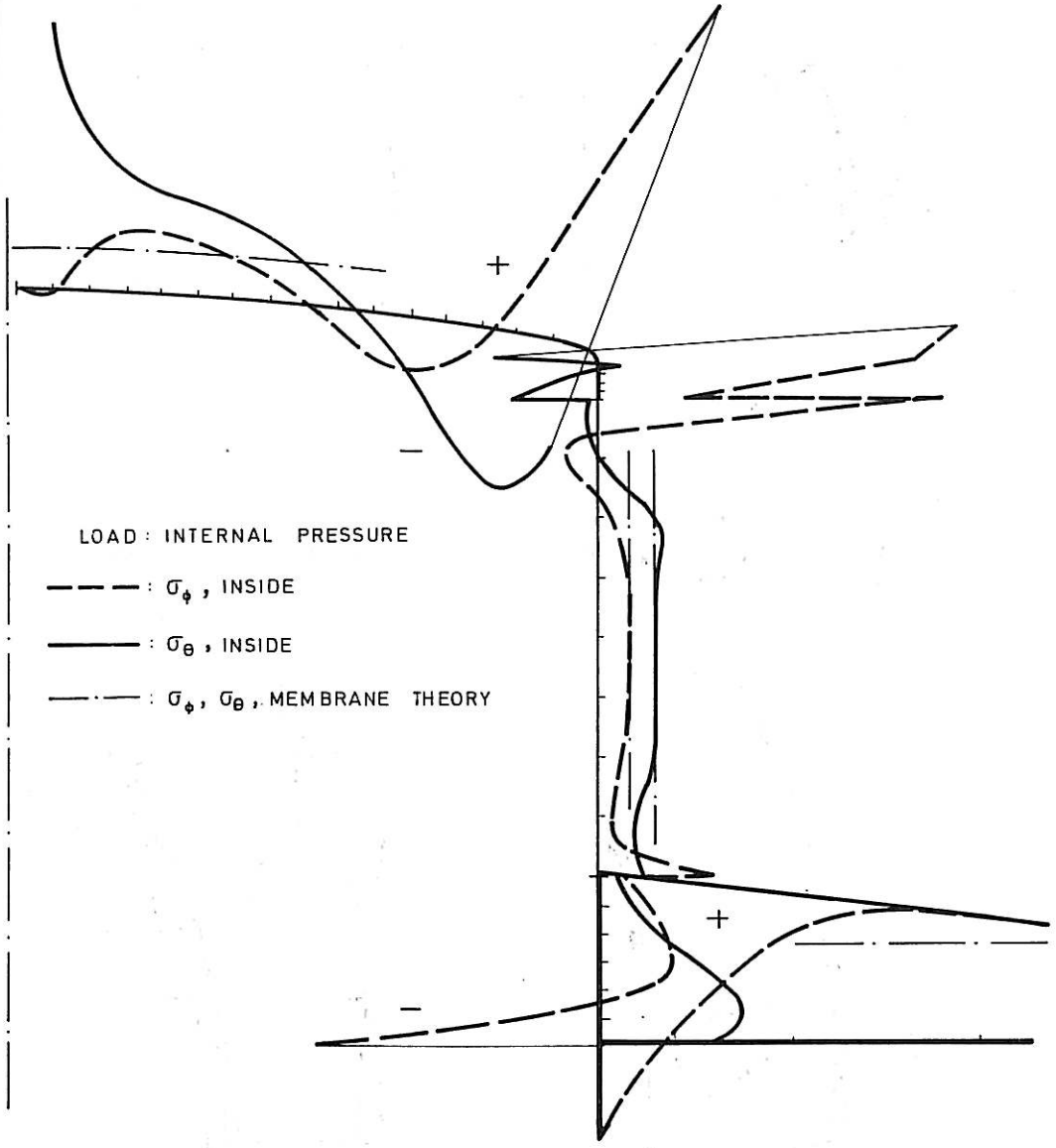

Fig. 36. Surface stresses in dome region. Load: internal pressure.

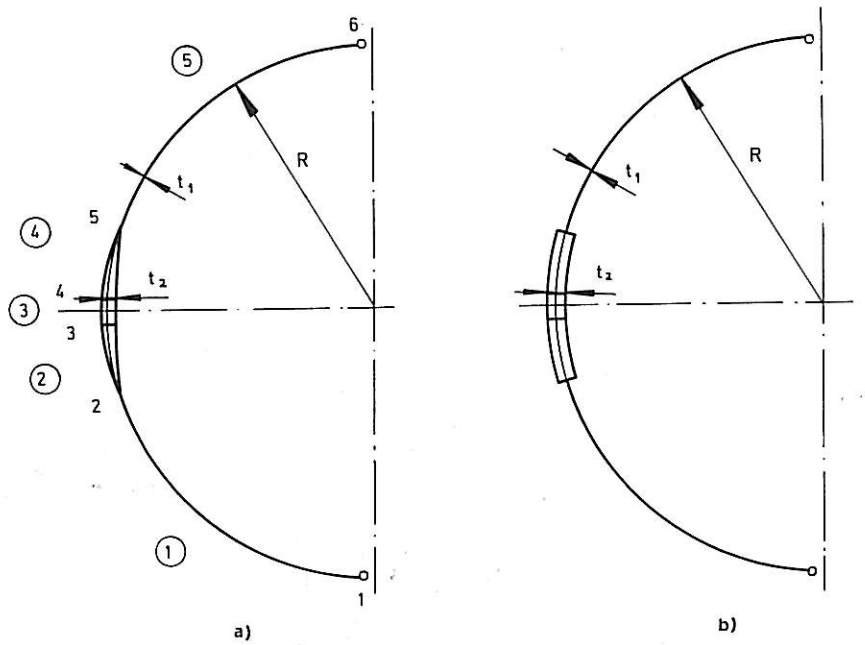

Fig. 37. Models used in calculating the effect at the transition between two plates with difference in plate thickness.

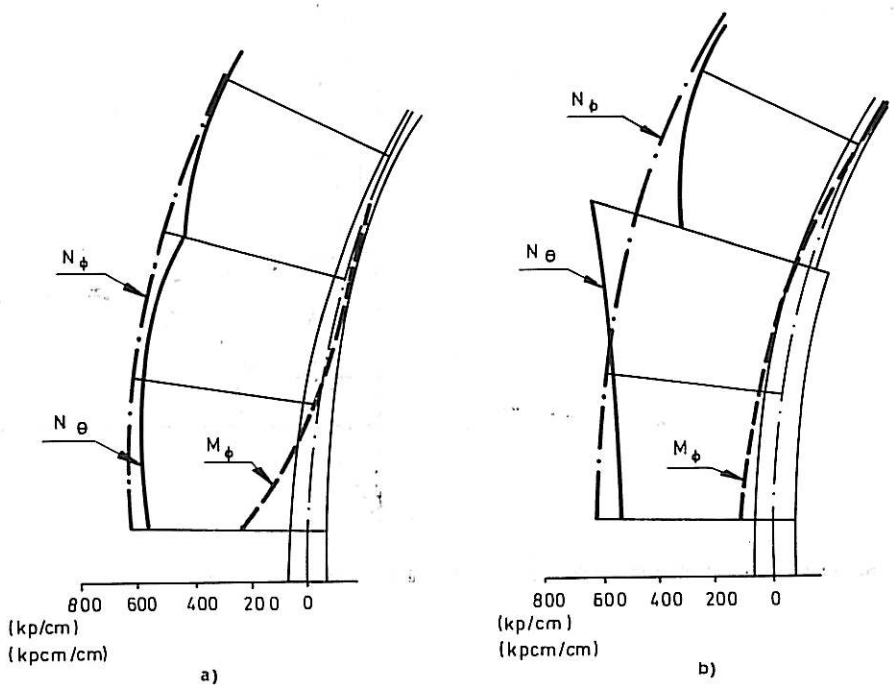

Fig. 38. Membrane forces and moments of the models in Fig. 37.

The whole sphere consists of 5 segments of the CIRCLE type. The relation between the different plate thicknesses, $t_2/t_1 = 1{,}212$.

In Fig. 38 membrane forces and moments are shown. N_ϕ is equal to $0{,}5pR$ according to membrane theory and is not influenced by moments and difference in plate thicknesses like N_θ.

Outside the equator area the moment rapidly approaches zero and a pure membrane condition occurs.

Computing time was approximately 26 seconds

Acknowledgements

The author wishes to express his thanks to Dipl.Eng. Odd Biberg of Kværner Brug A/S – Oslo who contributed Ch. 8 and to Det norske Veritas – Research Department – who contributed Ch. 9. Thanks are also due to A. Jespersen & Søn A/S of Copenhagen and to Apeland & Mjøset A/S – Oslo, for permitting use of the results presented in Sections 7.1 and 7.2, respectively.

Manuscript received 1973–01–10.

References

1. FLÜGGE, W., Stresses in shells. Berlin, Springer Verlag 1962.
2. BRØNDUM-NIELSEN, T., Axisymmetric bending of shells. Copenhagen, Danish Technical Press 1962.
3. BORN, J., Praktische Schalenstatik. Band I: Die Rotationschalen. Berlin, W. Ernst & Sohn 1968.
4. HARTUNG, R., An assessment of current capability for computer analysis of shell structures. Comput. Struct. 1(1971) 1/2, p. 3···32.
5. FALKENBERG, J.C., The general analysis of shells of revolution as applied to hyperbolic cooling towers under the action of wind forces and dead loads. Southampton 1966. [University of Southampton, Department of Civil Engineering.]
6. FALKENBERG, J.C., A method for integration of unstable systems of ordinary differential equations subject to two-point boundary conditions. BIT 8(1968) 2.
7. Report of the Committee of Inquiry into Collapse of Cooling Towers at Ferrybridge Monday 1. Nov. 1965. Central Electricity Generating Board, London 1966.

Appendix. Computer programme RSHELL – brief description

A.1 *General*

The following is a brief description of the RSHELL computer programme, currently running on a Univac 1108 installation in Oslo. For detailed information about input/output the reader is referred to the user's manual (in Norwegian), dated 1. November 1969, where a number of examples also appear. Inquiries should be directed to:

Norwegian Building Research Institute
Blindern, Oslo 3
Norway.

A.2 *Scope*

The present version of the programme will analyse a structure in the form of one or a number of adjoining shells of revolution which eventually have discrete stiffening rings between segments. The analysis will be performed in accordance with the theory presented in the preceding chapters. The example given in Ch. 8 will serve to illustrate the generality.

A.3 *Input*

The generating curve for the shell may consist of a number of segments of various forms such as

- straight lines
- circular arches
- parabolas, elipses, hyperbolas
- polynominal curves,(up to 4. order).

The shells may have linearly varying thickness between nodes, although there is no provision for anisotropic properties in the current version.

The boundary conditions may be specified at each end by the standard forms

- free
- fixed
- hinged
- ring
- symmetric
- special

where »symmetric» indicates a plane of symmetry normal to the shell axis. »Special» indicated a non-standard condition, e.g. of the form given in Section 4.7.

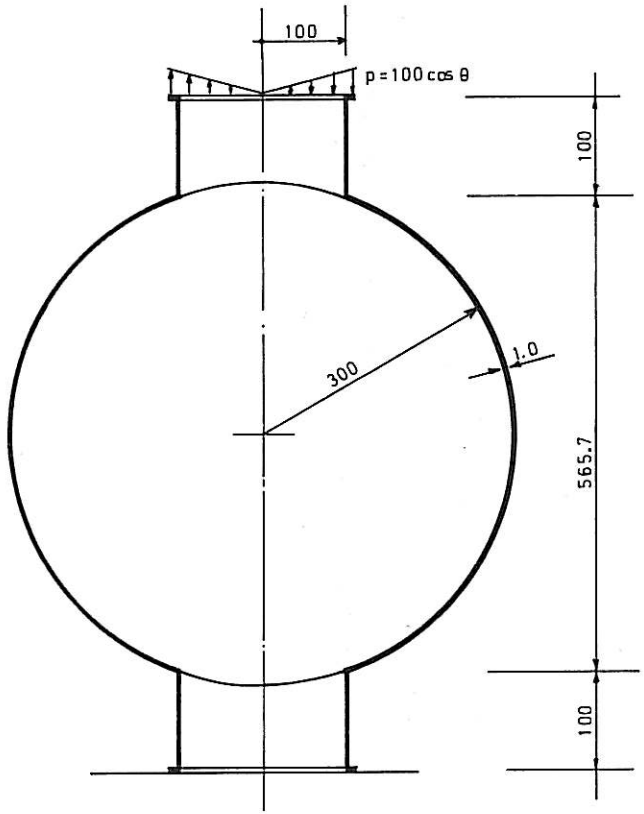


```
KULESKALL MED SYLINDRISKE TILSLUTNINGSPARTIER
GEOMETRY
NODECOORD 100. 0.  100.  100.   100. 665.689  100. 765.689
SEGTYPES BETWEEN NODES  1 2 1
RINGTYPES  1 1 AT NODES 1 4
SEGMENTS
EMODUL 2100000. POIS 0.3
SEGTYPE 1 LINE INTERVALS 4  T 1.0
SEGTYPE 2 CIRCLE  300.  INTERVALS 40 T 1.0
RINGS
EMODUL 2100000. POIS 0.3
RINGTYPE 1 RECTANGULAR   10.  2.  OUTSIDE
EDGES
EDGE 1 FIXED
EDGE 2 RING
PARAMETERS
SEGTYPE 1 NSUBX 14
SEGTYPE 2 IISUB 3 NSUBX 10
LOADS
RING LOAD PV 100. DISTRIBUTION 1 AT NODE 4
DEFINE DISTRIBUTION 1 FCOEFF 1 1.
OUTPUT
FOURIER TERMS
THETA POINTS  0.
PRINCIPAL STRESSES
COMPUTE
```

Fig. A.1. An example of input for the RSHELL programme.

Rings between segments with various cross-sectional shapes may be specified.
Loads may be specified, with proper direction, as

- dead load
- line load around an arbitrary circumference
- surface load over a part of the surface
- ring load on a ring.

The Fourier distribution for each load is specified separately.

A.4 *Output*

The desired output may be specified via input as follows:

- actions for each Fourier term separately
- actions for all Fourier terms combined
- principal forces
- principal stresses.

The points in the θ-direction at which output is wanted may also be specified (up to 13 points).

A.5 *Restrictions*

The current (1972) operating version is subject to the following restrictions:

- number of nodes $\leqslant 21$
- number of stations in s-direction $\leqslant 81$
- number of different segment types $\leqslant 10$
- number of different ring types $\leqslant 6$
- number of loads $\leqslant 20$
- number of Fourier terms $\leqslant 30$.

A.6 *Example*

Fig. A.1 shows the input for the analysis of a sphere with two adjoining cylinders, each stiffened by a ring and acted on by an asymmetrical load on the upper ring. The input is to a large extent self-explanatory, and the example is included with the intention of illustrating what is briefly described in the preceding paragraphs.